University of Stuttgart
Institute of Geodesy

Analysis of seasonal loading-induced displacements from GPS and GRACE

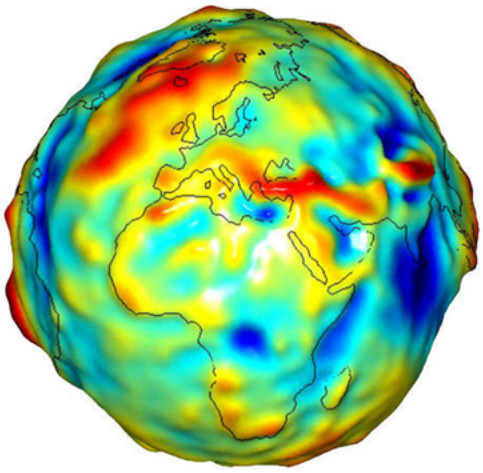

Master Thesis

GEOENGINE

at the University of Stuttgart

Jinwei Zhang

Stuttgart, February 2014

Supervisor: Prof. Dr.-Ing. Nico Sneeuw
University of Stuttgart

Qiang Chen, M.Sc.
University of Stuttgart

Erklärung der Urheberschaft

Ich erkläre hiermit an Eides statt, dass ich die vorliegende Arbeit ohne Hilfe Dritter und ohne Benutzung anderer als der angegebenen Hilfsmittel angefertigt habe; die aus fremden Quellen direkt oder indirekt übernommenen Gedanken sind als solche kenntlich gemacht. Die Arbeit wurde bisher in gleicher oder ähnlicher Form in keiner anderen Prüfungsbehörde vorgelegt und auch noch nicht veröffentlicht.

Ort, Datum Unterschrift

Acknowledgment

This thesis is completed under the careful supervision of Prof. Nico Sneeuw and Mr. Qiang Chen of University of Stuttgart. My deepest gratitude goes firstly and foremost to them, for their professional guidance, strong support and continuous encouragement. Without the consistent and illuminating instruction from Prof. Nico Sneeuw during the writting of the thesis, it could not have reached its present form. Without the patient guidance and invaluable advice from Mr. Qiang Chen, this research could not have progressed smoothly and been completed successfully.

Secondly, I would like to express my heartfelt gratitude to Mr. Balaji Devaraju, for providing me the GRACE data and giving me generous assistance on GRACE data processing. At the same time, I sincerely thank Prof. Wolfgang Keller for his kindly help and answering my questions. Additionally, I would also like to thank Prof. Wolfgang Keller for giving me useful suggestions on my work, and Mr. Lin Wang for kindly help on Matlab.

Furthermore, I am grateful to Dr. Rong Zou and Mr. Xavier Collilieux for providing me the processed GPS deformation time series, which contributes greatly to my research.

In addition, for professional teaching and patient answering countless questions, I would like to offer my sincere appreciation to the teachers who taught me during my master study in GEOENGINE program. Meanwhile, I would also thank my colleagues in the 6th GEOENGINE program and seniors from 5th generation, and the PhD fellows in the Institute of Geodesy, for their accompanying and selfless assistance in study and daily life.

Last but not least, my thanks would also go to my beloved parents for their boundless love and whole-hearted support during my study abroad over past two years in Germany.

Abstract

Mass transport within the Earth system over time (e.g., hydrological circulation) induces the mass redistribution on the surface. The temporal variation of mass load on the surface consequently leads to elastic deformation of Earth's surface (van Dam et al., 2001; Ilk et al., 2005; De Linage et al., 2007).

The surface deformation could be derived from GRACE through time-variable gravity field and also be observed by IGS stations in GPS 3D coordinates. The surface deformations derived from GRACE are spatially smoothed with about 350 km resolution. However, the deformations of IGS stations observed by GPS are discrete point measurements on the globe. Therefore, a validation of the consistency between the deformations from GRACE and GPS is necessary to be done, which would benefit the further research on mass transport and climate change.

In this study, using the data from GFZ, the deformations from GRACE are theoretically calculated in vertical and horizontal directions (Wahr et al., 1998; Kusche and Schrama, 2005). To investigate the disagreement between GPS and GRACE, a number of IGS stations in three regions are selected (i.e., Tibetan plateau, Danube basin and Great Lakes area) with period of 8 years (2003 – 2011). For a proper comparison, the spatial and temporal reference of GRACE and GPS need to be unified. For validation, the correlation coefficient, the Nash-Sutcliffe efficiency, and WRMS reduction are estimated.

After comparisons of deformation time series, almost all the stations in those regions show good consistency between GRACE and GPS in vertical component. There is distinct disagreement in horizontal component, probably due to the weak loading signals and strong local effects. Thus, several representative stations in those regions would be discussed and analyzed in detail.

Furthermore, to detect an optimal filter for GRACE, 40 IGS stations in Europe are involved to evaluate the filter performance. As a result, 52.5% stations filtered by the stochastic filter (i.e., Wiener filter) show better results, which indicates the optimal choice.

Key Words: GRACE, GPS, Surface deformation, Filter, Load variation, Mass transport, Gravity field, Satellite Geodesy.

Contents

List of Figures

List of Tables

Chapter 1

Introduction

1.1 Mass Transport and Mass Loading

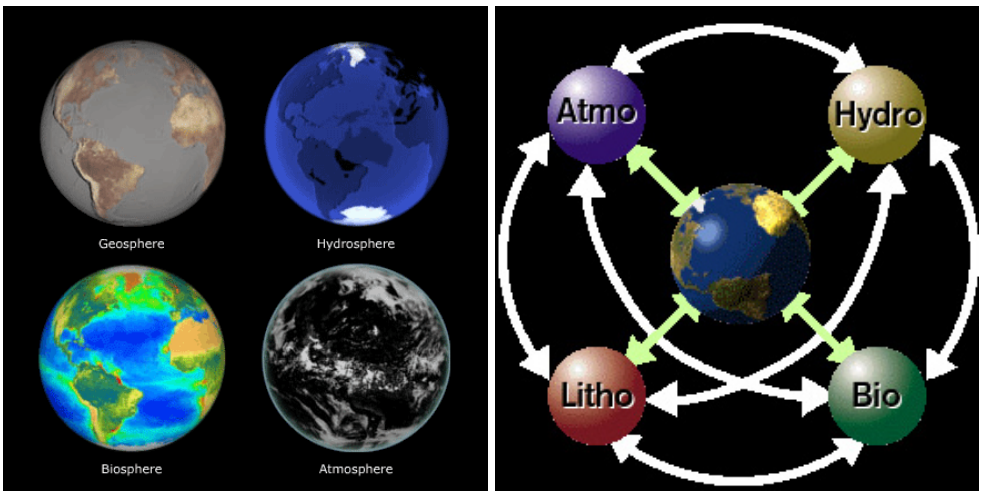

Figure 1.1: *Earth system: composed of four spheres* [1]

Earth system is composed of several components: the solid Earth, hydrosphere, atmosphere, lithosphere and biosphere. Although the whole Earth system is conservative and the mass of Earth system remains the same all the time, masses are transported and redistributed in and among different parts of Earth. With the interaction and interchange among the hydrosphere, atmosphere, lithosphere, biosphere and solid Earth in various ways, the mass variation occurs on all temporal and spatial scales (daily, monthly, seasonally, interannually, decadally, etc.).

For instance, the circulation in the ocean and in the atmosphere may cause the sea level change as a result of the ocean current; Water fluxes between continental water storages may induce the surface load variation, which causes the temporal change of Earth's surface shape; Glacial ice melting is also one of the reasons for surface mass variation. Not only the mass transport

[1] http://serc.carleton.edu/eslabs/climate/1a.html
http://serc.carleton.edu/introgeo/earthsystem/nutshell/courses.html

driven by the hydrological cycle, but also other processes such as tectonic motions, volcanic processes, and other geodynamic processes can influence the mass transport and redistribution as well (Ilk et al., 2005).

With the knowledge of the mass distribution and redistribution within the Earth system, the exploration of the geodynamic convective and climatologically driven processes can be realized, which is so significant to understand and model the global geodynamics within the Earth system. That will definitely help us model the actual Earth and investigate the Earth dynamics. Furthermore, that is crucial to estimate the climate changes, especially the global hydrological cycle (Ilk et al., 2005).

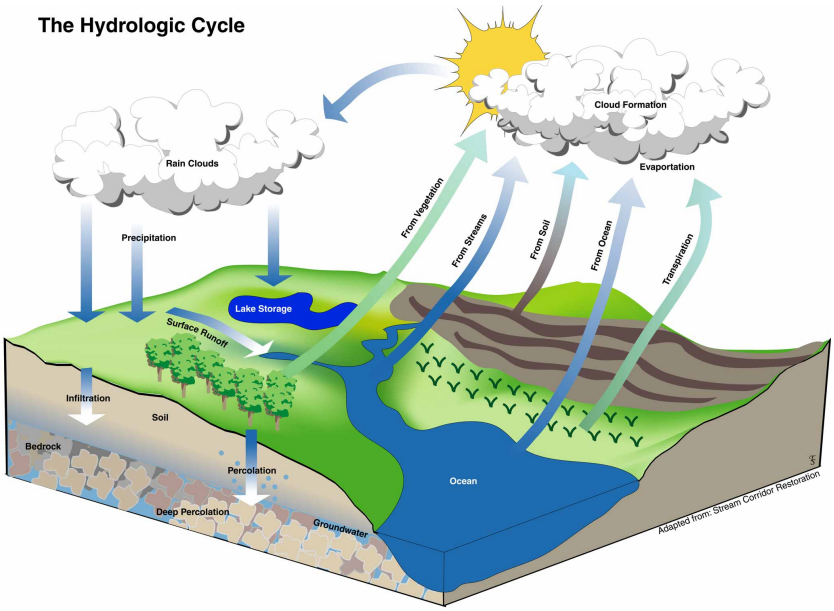

Figure 1.2: *Hydrologic cycle on the Earth* [2]

Since the masses transport within the Earth system over time, those induce the mass redistribution on the globe. Hence, the load of masses on the surface consequently varies, which contributes to the temporal variation of gravity. Because the geoid of Earth is defined as an equipotential surface of gravity, the variation of gravity would influence the height displacements. Therefore, the surface loading variation caused by mass redistribution consequently leads to the elastic displacements on the Earth's surface (van Dam et al., 2001; De Linage et al., 2007).

As we know, the mass load gives pressure on the surface due to the gravitation. As a result of load variation, the surface displacements occur primarily in the vertical direction, which is clearly shown in Figure 1.4. And also, the displacements theoretically occur in the horizontal direction. As is described graphically, after the the continental water loads on, the station moves to a new location, and then rebounds back to the original location if the water load is

[2] http://www.buffer.forestry.iastate.edu/Photogallery/illustrations/illustrations-1.html

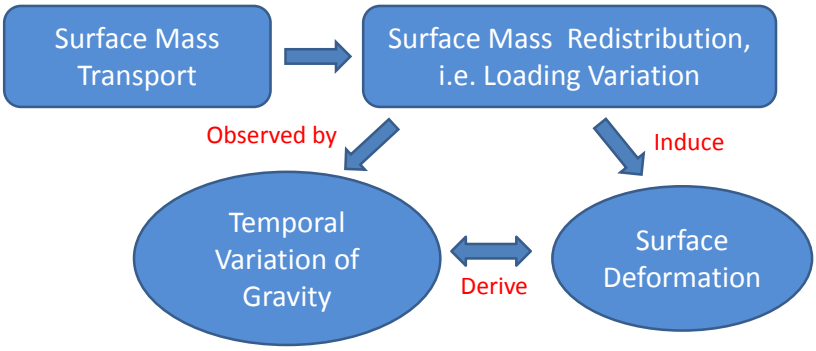

Figure 1.3: *Process of mass transport and loading variation*

removed. Because of the hydrological cycle, the continental water load varies obviously on the Earth's surface. The elastic displacements here are regarded mainly as the result of hydrological loading variations.

Considering all the effects coming from atmosphere and ocean as well as other effects like tectonics, the analysis of the causes of the surface displacements may become much more complicated. Sometimes one can deduce the sources of the influence via their periodical behaviour.

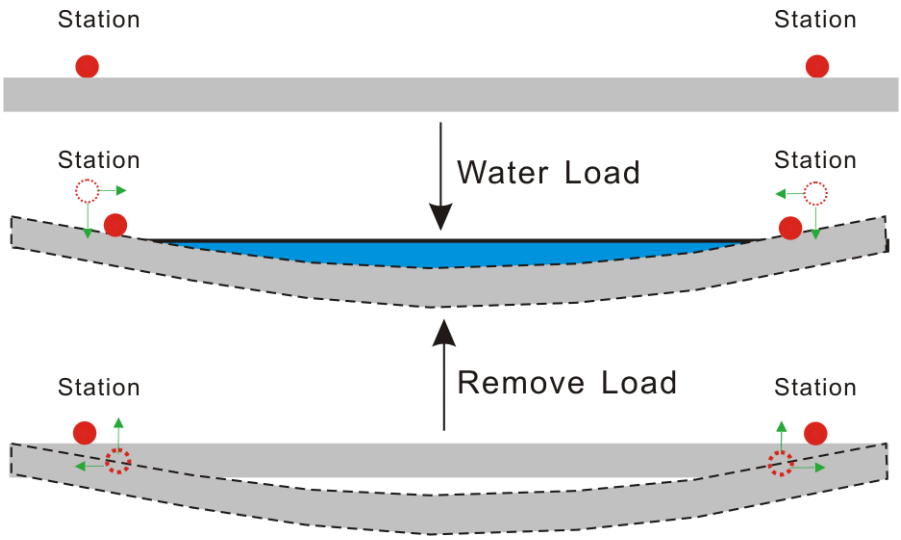

Figure 1.4: *Loading variation effects on surface displacements*

1.2 Motivation

People always wonder and would like to know what the real Earth is and how it changes over time. Due to the development of satellite technology and the improvement of geodetic observation sensors, several gravity satellite missions are successively launched, such as CHAMP,

GRACE, GOCE, etc. The global static and time-variable gravity field is able to be observed by those satellite missions with unprecedented accuracy. Therefore, it is then possible to monitor the geometric deformation of the shape of Earth caused by the mass variation and redistribution.

By observing the change of the Earth's gravity field, the deformation of the Earth's surface can be derived theoretically from gravity changes if loading theory is applied (Wahr et al., 1998). In this way, we can analyze how the shape of Earth changes globally and regionally. Conversely, if the temporal surface displacements are observed, Earth's gravity field changes could also be inversely determined, and the surface mass loading variation could consequently be estimated.

Using GPS station coordinates, the surface deformations can be observed, too. Therefore, it is possible to combine GPS with GRACE to measure the surface displacements (van Dam et al., 2007; Davis et al., 2004; Tesmer et al., 2011; Fu and Freymueller, 2012; Fu et al., 2012) or to deduce the surface loading variation (Kusche and Schrama, 2005; Jansen et al., 2009; Nahmani et al., 2012; Rietbroek et al., 2012). A validation of combining both observation techniques is necessary to be done before further analysis.

When GPS and GRACE are combined together, the inconsistency of spatial and temporal resolutions of GPS and GRACE should be taken into account. The surface displacements calculated from GRACE data are spatially smoothed with about 350 km resolution. However, the deformations of IGS stations observed by GPS are discrete point measurements on the Earth. Thus, the incomparability issue needs to be solved before we compare GPS with GRACE with each.

1.3 Objectives and Outline

1.3.1 Objectives

As is described above, temporal variation of mass may cause the geographic redistribution of the surface loading, which then induces the elastic surface displacements. Thus, in the thesis, our research mainly focus on:

- Investigating elastic surface displacements caused by surface loading in vertical/radial and horizontal/lateral directions. The surface displacements can be derived from GRACE time-variable gravity field coefficients as well as be observed by GPS 3D coordinates of IGS stations.

- Analyzing the performance of two different geodetic observation techniques on deformation monitoring in three different regions. GRACE observes the mass variation so

that the gravity field changes measured by GRACE can be turned into surface elastic displacements, while GPS measures the geometric coordinate changes, that both of them are potentially capable to monitor the surface displacements.

- Evaluating the disagreement of deformation time series between GPS and GRACE. The deformation time series we compared here come from two completely different observation methods, e.g. different temporal and spatial resolutions.

  Based on comparisons, a successful validation can be affirmed if the deformation time series derived from GRACE are nearly consistent over time with deformation time series observed by GPS.

- Evaluating the filter behaviour on GRACE-derived deformation time series. Filtering is always very important, especially for GRACE data. To test the filter sensitivity is not our main goal but still necessary, so that we can know how much the filtering influences the analysis of loading caused surface displacements in the time domain and then obtain the optimal filter scheme by comparing with displacements from GPS.

1.3.2 Outline

Chapter 2 (Satellite Missions) contains an overview of three different satellite missions, a detailed introduction of GRACE mission including its instruments on board, operation principle and mission objectives, and a short introduction of GPS global tracking network.

Chapter 3 (Methodology) is the kernel part of the thesis, that explains the data processing procedure. It theoretically introduces the methods we use to derive the surface displacements from GRACE time-variable gravity field, including the mathematical fundamentals of spherical harmonic approach, the way to unify the spatial and time reference frame. It also discusses different kinds of filters, which will be applied in GRACE data processing. Besides that, it introduces the statistical methods used in following data analysis.

Chapter 4 (Data Analysis) principally interprets the results, analyzes the surface displacements in three different regions, statistically evaluates the disagreement of deformation time series between GRACE and GPS as well as the filter sensitivity test.

Chapter 5 (Summary) briefly summarizes the thesis work, draws the conclusions and provides an outlook.

Chapter 2

Satellite Missions

2.1 Overview of Satellite Missions

The first gravity satellite mission is CHAllenging Mini-Satellite Payload for Geosciences and Application (CHAMP), which was designed as a geodesy satellite, is produced and launched by German Research Center for Geoscience (GFZ) on Jul. 15, 2000. The CHAMP mission terminated on Sept. 19, 2010 after more than ten years of operation. The orbit information of satellite are listed in Table 2.1.

With the improvement of the satellite orbit tracking technology, the orbits of satellites could be determined more accurately. That makes it possible to recover the gravity field through analysis of precise satellite orbits. As CHAMP used the high-low Satellite-to-Satellite Tracking (hl-SST) technique, it could obtain a better global gravity field of Earth than ever by other observation techniques (e.g. Satellite Laser Ranging (SLR)). It thus made a great progress in satellite geodesy and physical geodesy (Reigber et al., 2002).

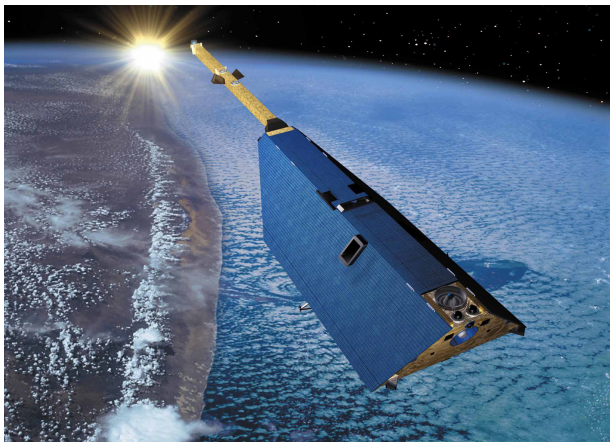

Figure 2.1: *CHAMP mission* [1]

[1] http://www.dlr.de/rd/en/

Table 2.1: *Parameters of CHAMP and GOCE orbits*

	CHAMP	GOCE
Altitude	445 km	about 250 km
Eccentricity	near-circular	near-circular
Inclination	87.18 °	96.7 ° (sun-synchronous)
Period	93.55 minutes	90.14 minutes

The second gravity satellite mission is called Gravity Recovery And Climate Experiment (GRACE), which was launched on March 17, 2002. Different from CHAMP, the GRACE mission, which consists of two satellites in a same orbit, uses both hl-SST and low-low Satellite-to-Satellite Tracking (ll-SST) technology.

With such advantages, GRACE provides much better accuracy in long- and medium-wavelength than CHAMP in gravity field determination, improving the model of gravity field up to harmonic degree and order 180 (Tapley et al., 2004; Tapley, 2007). By means of time-variable gravity field determination, GRACE can provide valuable information on the mass distribution variation over the Earth, advancing satellite geodesy and geodynamics beyond CHAMP.

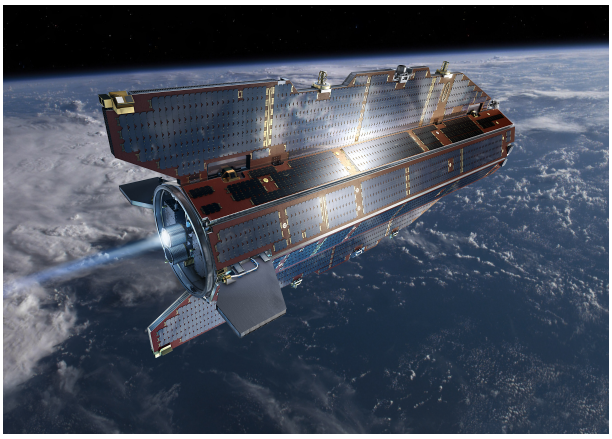

Figure 2.2: *GOCE mission* [2]

For GRACE, since it can measure the time-variable gravity field and monitor the variation of mass distribution, it could be applied in analysis of load redistribution and surface displacements. In this thesis, GRACE data are used to derive surface displacements for comparisons with GPS deformation time series. Thereby, the GRACE mission will be specified in the following section.

[2]http://portal.tugraz.at/portal/page/portal/Files/i5210/images/GOCE/6.jpg

After the launch of GRACE, a new gravity satellite mission, named Gravity Field and Steady-State Ocean Circulation Explorer (GOCE), was launched by the European Space Agency (ESA) in a low Earth orbit. The orbit information of satellite are in Table 2.1.

Carrying a extremely sensitive gravity gradiometer on board, GOCE is able to determine gravity anomaly with an accuracy of only 1 mGal, and with spatial resolution of 100 km (LeGrand and Minster, 1999; Drinkwater et al., 2006). Because of its high spatial resolution and high accuracy of gravity anomaly, it performs a better results of static Earth's gravity field.

GOCE has come down in October 2013, and a magnetic satellite mission called Swarm has been already launched in November 2013, and a GRACE Follow-on has also been planned in 2017.

2.2 GRACE Mission

2.2.1 General Information

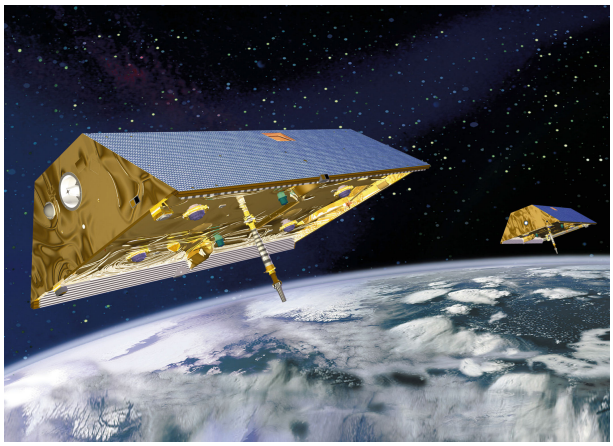

Figure 2.3: *GRACE mission* [3]

GRACE is a joint project among the National Aeronautics, the Space Administration (NASA) and the German Aerospace Center (DLR) (Case et al., 2002). The mission has been proposed in 1996 jointly by the University of Texas at Austin, Center for Space Research (UTCSR), involving the German Research Centre for Geosciences (GFZ) and the Jet Propulsion Laboratories (JPL) in Pasadena, who is responsible for the overall mission management under the NASA Earth System Science Pathfinder (ESSP) program [4].

Different from CHAMP and GOCE, the GRACE mission consists of a pair of satellites flying in a low Earth orbit about 220 km apart from each other (Tapley et al., 2004). Although the

[3] http://pattyjansen.com/2011/11/29/looking-at-the-earth-through-different-eyes-the-grace-mission/
[4] http://www.csr.utexas.edu/grace/overview.html

Table 2.2: *Overview of GRACE mission*

Launch date	17 March 2002
Launch site	Plesetsk, Russia
Orbit Altitude	450–500 km
Orbit inclination	89 °
Mass	2× 487 kg
Length	2× 3.1 m
Mission lifetime	5 years (designed)

designed mission lifetime was only five years, the satellites have already operated for 11 years and still work today.

GRACE can monitor how mass is distributed around the Earth and how it varies over time. GRACE observations play the role of studying Earth's ocean, hydrology, and climate.

2.2.2 Instruments and Principle

Both GRACE satellites are equipped with the following instruments on board (NASA, 2002) (Dunn et al., 2002):

- K-Band Ranging System (KBR)
- Accelerometer (ACC)
- GPS Space Receiver (GPS)
- Laser Retro-Reflector (LRR)
- Star Camera Assembly (SCA)
- Coarse Earth and Sun Sensor (CES)
- Ultra Stable Oscillator (USO)
- Center of Mass Trim Assembly (CMT)

The Star Camera Assembly (SCA) (as for CHAMP) is used for the precise orientation of the satellite within the AOCS and for the correct interpretation of the ACC measurements.

The accelerometer (ACC) serves to measure all non-gravitational accelerations on the GRACE satellite due to air drag, solar radiation pressure or attitude control activator impulses initiated by the attitude and orbit control system (AOCS).

To consider precise attitude and non-gravitational forces, both satellites are equipped with star cameras and accelerometers.

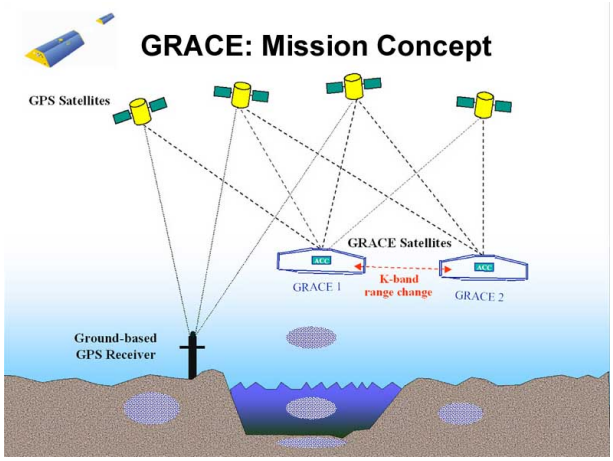

Figure 2.4: *Illustration of the operation principle of GRACE mission* [5]

The position and velocity of the satellites is measured by using onboard GPS antennae and (for validation purposes) SLR retro-reflectors. The GPS TurboRogue Space Receiver receiver assembly provided by JPL serves for Precise Orbit Determination (POD) with cm-accuracy, and time tagging of all payload data. To achieve these goals, hl-SST between the GRACE and the high-altitude orbiting GPS satellites is performed.

Additionally, to measure the exact separation distance and its rate of change to an accuracy of better than 0.1 μm/s, the K-band ranging (KBR) system is the key scientific instrument of GRACE which measures the dual one-way range change between both satellites with a precision of about 1 μm/s.

The GRACE mission uses KBR system to accurately measure changes in the speed and distance between two identical spacecraft flying in a polar orbit about 220 kilometers apart above Earth. The KBR system is sensitive enough to detect separation changes as small as 10 mm over a distance of 220 kilometers.

Depending on the ll-SST by KBR and hl-SST by GPS receivers on board, the orbit perturbations and precise position of satellites can be accurately observed. Combining with the 3D ACC and SCA, GRACE is able to make accurate measurements of the distance between the two satellites.

As a consequence, the Earth's gravity field can be determined. It provides scientists from all over the world with an efficient and cost-effective way to map the Earth's gravity fields. The results from GRACE can present significant information about the distribution and flow of mass within and around the Earth.

[5] http://www.csr.utexas.edu/grace/publications/presentations/HPC2001.html

In combination with the sub-millimeter intersatellite distance observed by the K-band ranging system (KBR) and the accurate satellite position measured by the onboard GPS receiver, the Earth's gravity field can be deduced with unprecedented accuracy.

2.2.3 Mission Objectives

The primary scientific objective of the GRACE mission is to measure the Earth's gravity field and its time variability with unprecedented accuracy.

Also, GRACE provides the time variability of the Earth's overall external shape, the geoid. Consequently, since its launch in March 2002, this fundamental dataset has enabled dramatic improvements of seasonal and inter-annual climate change estimates.

The secondary task of the GRACE mission is to keep a daily record of several hundred globally distributed profiles of the delay or inclination angle of GPS measurements. Both can be converted into a total electron or refractivity by applying Atmospheric- and Ionospheric-Profiling (NASA, 2002).

Accordingly, the GRACE mission could be applied on monitoring changes in continental water storage, determining variation in ocean bottom pressure, measuring the redistribution of mass, and monitoring the variation of ice and snow melting (Rodell and Famiglietti, 2001; Velicogna and Wahr, 2005; Seo et al., 2006).

2.3 GPS Global Network

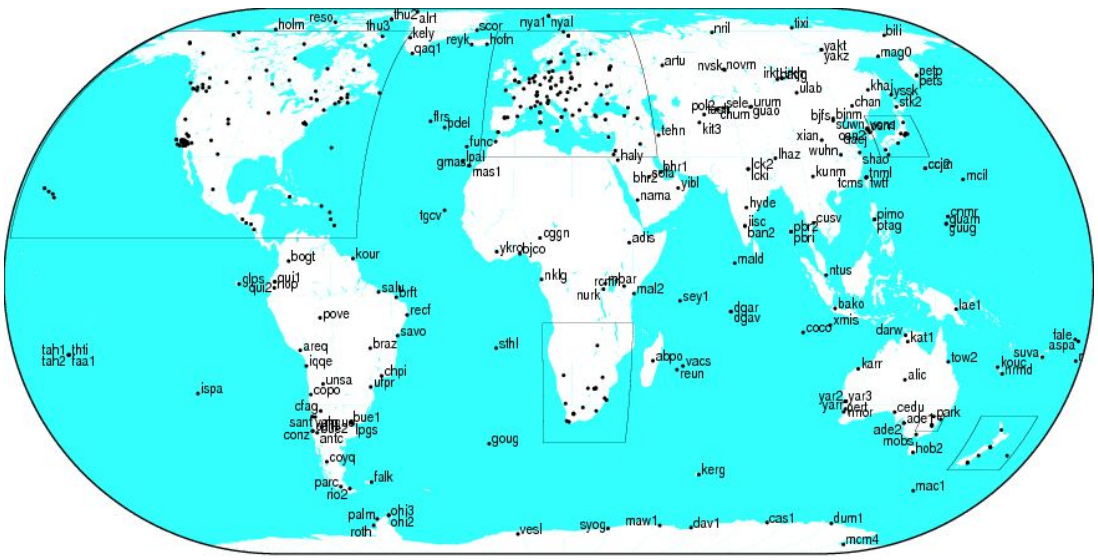

Figure 2.5: IGS global tracking network [6]

The International Global Navigation Satellite System Service (IGS) is a voluntary federation of more than 200 worldwide agencies and research groups that pool resources and permanent GPS and GLONASS station data to generate precise GPS and GLONASS products. The IGS is committed to providing the highest quality data and products as the standard for Global Navigation Satellite Systems (GNSS) in support of Earth science research, multidisciplinary applications, and education (*http://igscb.jpl.nasa.gov/network/netindex.html*).

To accomplish its goals, the IGS service members operate an international network of over 350 continuously operating dual-frequency GPS stations, more than a dozen regional and operational data centers, three global data centers, seven analysis centers and a number of associate or regional analysis centers. The global tracking network and network in Europe shown in Fig 2.5 and 2.6.

In this thesis, we choose the IGS stations in three different regions (Danube basin, Tibetan plateau and the Great Lakes area) on the Earth and use the long-term precise position information of IGS stations for seasonal deformation analysis.

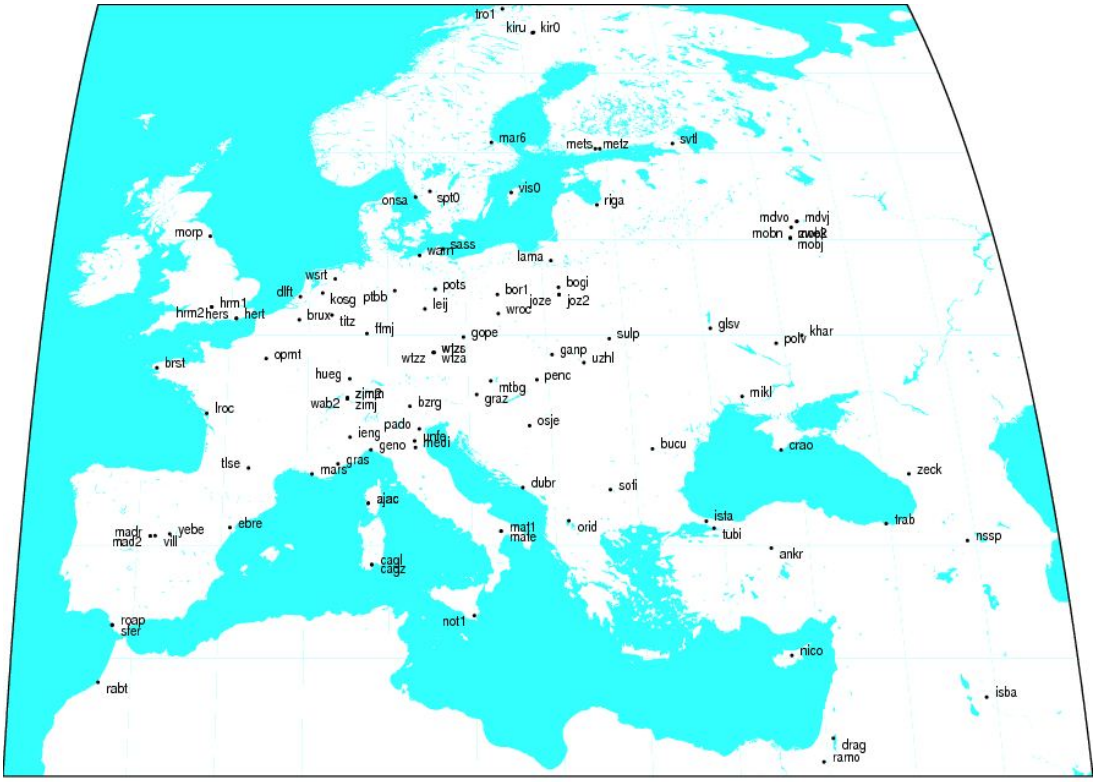

Figure 2.6: *IGS tracking network in Europe* [7]

[6]http://igscb.jpl.nasa.gov/network/complete.html
[7]http://igscb.jpl.nasa.gov/network/complete.html

Chapter 3

Methodology

3.1 Deformations due to Load Variation

3.1.1 Representation of Gravity Field

The gravitational potential in outer space can be described as a Laplace field, which has no divergence and is conservative. So the gravitational potential outside the Earth satisfied the Laplace equation:

$$\Delta V = 0 \,, \tag{3.1}$$

where the V is the gravitational potential and Δ is the Laplace operator.

The solutions of this equation are called harmonic functions, and formulated by a series of base functions. The Laplace equation can be solved both in Cartesian coordinates and spherical coordinates, e.g. in spherical coordinates the Laplace equation reads (Hofmann-Wellenhof and Moritz, 2005):

$$\Delta V = \frac{\partial^2 V}{\partial r^2} + \frac{2}{r} \cdot \frac{\partial V}{\partial r} + \frac{\cot\theta}{r^2} \cdot \frac{\partial V}{\partial \theta} + \frac{1}{r^2} \cdot \frac{\partial^2 V}{\partial \theta^2} + \frac{1}{r^2 \sin^2\theta} \cdot \frac{\partial^2 V}{\partial \lambda^2} \,, \tag{3.2}$$

where

- r is the spherical radius
- θ is the polar distance
- λ is the geocentric longitude

Leaving out the radial part, the base functions of the Laplace equation expressed in spherical coordinates are so called surface spherical harmonics:

$$Y_{lm}(\theta,\lambda) = P_{lm}(\cos\theta)\cdot\begin{pmatrix}\cos m\lambda\\ \sin m\lambda\end{pmatrix}, \tag{3.3}$$

where P_{lm} is the Legendre function.

Consequently, because of the spatial harmonic behaviors in outer space of Earth, the solutions of the Laplace equation of the gravitational field (Sneeuw, 2006) finally can be represented based on equation (3.7) by:

$$V(r,\theta,\lambda) = \frac{GM}{R}\sum_{l=0}^{\infty}\left(\frac{R}{r}\right)^{(l+1)}\sum_{m=0}^{l}\bar{P}_{lm}(\cos\theta)(\bar{C}_{lm}\cos m\lambda + \bar{S}_{lm}\sin m\lambda)\,, \tag{3.4}$$

where

- r is the spherical radius
- θ, λ are spherical coordinates
- l,m are degree and order
- GM is the gravitational constant
- R is the Earth's radius
- $\bar{P}_{lm}(\cos\theta)$ is normalized Legendre function
- $\bar{C}_{lm}$, $\bar{S}_{lm}$ are the normalized dimensionless spherical harmonic coefficients of degree l and order m

with

$$\bar{P}_{lm}(\cos\theta) = N_{lm}\cdot P_{lm}(\cos\theta) \tag{3.5}$$

$$N_{lm} = \sqrt{(2-\delta_{m,0})(2l+1)\frac{(l-m)!}{(l+m)!}}\,. \tag{3.6}$$

Normally, the general function on the surface of sphere can be expressed as a series of surface spherical harmonics (Hofmann-Wellenhof and Moritz, 2005) by:

$$f(\theta,\lambda) = \sum_{l=0}^{\infty}\sum_{m=0}^{l}P_{lm}(\cos\theta)(a_{lm}\cos m\lambda + b_{lm}\sin m\lambda) \tag{3.7}$$

with Legendre function P_{lm} and spherical harmonic coefficients a_{lm}, b_{lm}.

According to the two-dimensional Fourier transformations (Sneeuw, 1994), the surface spherical harmonics synthesis can be performed in two steps:

$$\begin{pmatrix} A_m(\theta) \\ B_m(\theta) \end{pmatrix} = \sum_{l=m}^{\infty} P_{lm}(\cos\theta) \begin{pmatrix} a_{lm} \\ b_{lm} \end{pmatrix} , \tag{3.8}$$

$$f(\theta, \lambda) = \sum_{m=0}^{\infty} [A_m(\theta) \cos m\lambda + B_m(\theta) \sin m\lambda] . \tag{3.9}$$

Equations are 1-dimensional Fourier transformations along the latitude, which can be seen in longitude direction. And the equation can be regarded obviously as a discrete Fourier series.

To improve the efficiency of global spherical harmonic computation, the two-dimensional Fourier methods would be applied in derivation of the deformations from GRACE in the thesis.

3.1.2 Deformations Derivation in Vertical and Horizontal Direction

Similar to equation (3.4), the gravity field information from GRACE is commonly represented in terms of the shape of the geoid N as a sum of spherical harmonics (Wahr et al., 1998), which reads:

$$N(\theta, \lambda) = R \cdot \sum_{l=0}^{\infty} \sum_{m=0}^{l} \bar{P}_{lm}(\cos\theta)(\bar{C}^{g}_{lm} \cos m\lambda + \bar{S}^{g}_{lm} \sin m\lambda) , \tag{3.10}$$

where R is the mean radius of the Earth, C^{g}_{lm} and S^{g}_{lm} are dimensionless spherical harmonic coefficients of disturbing potential, which is the difference between the coefficients of the real potential and normal potential. $\bar{P}_{lm}$ are normalized associated Legendre functions.

Considering the time-dependent changes in geoid, ΔN could be either considered as the change in N from one time to another, or the difference between N at one time and a time average of N. So ΔN could be expressed in terms of the spherical harmonic coefficients of geoid change $\Delta C^{g}_{lm}, \Delta S^{g}_{lm}$ as

$$\Delta N(\theta, \lambda) = R \cdot \sum_{l=0}^{\infty} \sum_{m=0}^{l} \bar{P}_{lm}(\cos\theta)(\Delta C^{g}_{lm} \cos m\lambda + \Delta S^{g}_{lm} \sin m\lambda) . \tag{3.11}$$

In the thesis, we consider the Earth system as a composition of two parts: a spherical solid Earth and surface mass which is free to redistribute in a thin surface layer of surface density. So we also parameterize the surface mass density change $\Delta\sigma$ as a sum of spherical harmonics (Wahr et al., 1998)

$$\Delta\sigma(\theta, \lambda) = R\rho_w \cdot \sum_{l=0}^{\infty} \sum_{m=0}^{l} \bar{P}_{lm}(\cos\theta)(\Delta C^{\sigma}_{lm} \cos m\lambda + \Delta S^{\sigma}_{lm} \sin m\lambda) . \tag{3.12}$$

Here C^{σ}_{lm} and S^{σ}_{lm} represent the spherical harmonic coefficients of the surface density anomaly. ρ_w is the density of water and it is included here in order that C^{σ}_{lm} and S^{σ}_{lm} are dimensionless.

To obtain the surface deformations, Mitrovica et al. (1994) has outlined a spectral formalism for computing 3D deformations from surface mass loading. The mathematical relationships between vectorial surface displacements and spherical harmonic coefficients of surface 3D changes are proposed by Kusche and Schrama (2005):

$$dH(\theta,\lambda) = R \cdot \sum_{l=0}^{\infty} \sum_{m=0}^{l} \bar{P}_{lm}(\cos\theta)(\Delta C^{h}_{lm} \cos m\lambda + \Delta S^{h}_{lm} \sin m\lambda) \tag{3.13}$$

$$dE(\theta,\lambda) = \frac{R}{\sin\theta} \cdot \sum_{l=0}^{\infty} \sum_{m=0}^{l} m\bar{P}_{lm}(\cos\theta)(-\Delta C^{\psi}_{lm} \sin m\lambda + \Delta S^{\psi}_{lm} \cos m\lambda) \tag{3.14}$$

$$dN(\theta,\lambda) = -R \cdot \sum_{l=0}^{\infty} \sum_{m=0}^{l} \frac{\partial}{\partial\theta}\bar{P}_{lm}(\cos\theta)(\Delta C^{\psi}_{lm} \cos m\lambda + \Delta S^{\psi}_{lm} \sin m\lambda)\,. \tag{3.15}$$

dH represents height deformation, and dE, dN are lateral deformations in east and north direction. ΔC^{h}_{lm}, ΔS^{h}_{lm} indicate the spherical harmonic coefficients of height deformations, and ΔC^{ψ}_{lm}, ΔS^{ψ}_{lm} are the spherical harmonic coefficients of the lateral deformations.

According to Farrell's loading theory (Farrell, 1972), the changes of the spherical harmonic coefficients of the surface density can be related to the spherical harmonic coefficients of the geoid changes, vertical deformations and horizontal deformations through the load Love numbers. Hence, the surface mass variation is linked with surface displacements in vertical and horizontal direction:

$$\Delta C^{g}_{lm} = \frac{3\rho_w}{\rho_e}\frac{1+k'_l}{2l+1}\Delta C^{\sigma}_{lm} \tag{3.16}$$

$$\Delta C^{h}_{lm} = \frac{3\rho_w}{\rho_e}\frac{h'_l}{2l+1}\Delta C^{\sigma}_{lm} \tag{3.17}$$

$$\Delta C^{\psi}_{lm} = \frac{3\rho_w}{\rho_e}\frac{l'_l}{2l+1}\Delta C^{\sigma}_{lm} \tag{3.18}$$

and

$$\Delta S^{g}_{lm} = \frac{3\rho_w}{\rho_e}\frac{1+k'_l}{2l+1}\Delta S^{\sigma}_{lm} \tag{3.19}$$

$$\Delta S^h_{lm} = \frac{3\rho_w}{\rho_e}\frac{h'_l}{2l+1}\Delta S^\sigma_{lm} \tag{3.20}$$

$$\Delta S^\psi_{lm} = \frac{3\rho_w}{\rho_e}\frac{l'_l}{2l+1}\Delta S^\sigma_{lm}\,, \tag{3.21}$$

where k'_l, h'_l, l'_l are load Love numbers.

From the equations above, we can derive the relationship between ΔC^h_{lm} and ΔC^g_{lm} as well as between ΔC^ψ_{lm} and ΔC^g_{lm}, then

$$\Delta C^h_{lm} = \frac{h'_l}{1+k'_l}\Delta C^g_{lm} \tag{3.22}$$

$$\Delta C^\psi_{lm} = \frac{l'_l}{1+k'_l}\Delta C^g_{lm}\,, \tag{3.23}$$

and the same transformation would be given in height direction for ΔS^h_{lm} and ΔS^g_{lm}, and in lateral direction for ΔS^ψ_{lm} and ΔS^g_{lm}

$$\Delta S^h_{lm} = \frac{h'_l}{1+k'_l}\Delta S^g_{lm} \tag{3.24}$$

$$\Delta S^\psi_{lm} = \frac{l'_l}{1+k'_l}\Delta S^g_{lm}\,. \tag{3.25}$$

Combining equation (3.13) – (3.25) shown above, we can finally derive the 3D displacements in terms of ΔC^g_{lm} and ΔS^g_{lm},

$$dH(\theta,\lambda) = R\cdot\sum_{l=0}^{\infty}\sum_{m=0}^{l}\bar{P}_{lm}(\cos\theta)(\Delta C^g_{lm}\cos m\lambda + \Delta S^g_{lm}\sin m\lambda)\frac{h'_l}{1+k'_l} \tag{3.26}$$

$$dE(\theta,\lambda) = \frac{R}{sin\theta}\cdot\sum_{l=0}^{\infty}\sum_{m=0}^{l}m\bar{P}_{lm}(\cos\theta)(-\Delta C^g_{lm}\sin m\lambda + \Delta S^g_{lm}\cos m\lambda)\frac{l'_l}{1+k'_l} \tag{3.27}$$

$$dN(\theta,\lambda) = -R\cdot\sum_{l=0}^{\infty}\sum_{m=0}^{l}\frac{\partial}{\partial\theta}\bar{P}_{lm}(\cos\theta)(\Delta C^g_{lm}\cos m\lambda + \Delta S^g_{lm}\sin m\lambda)\frac{l'_l}{1+k'_l} \tag{3.28}$$

As we normally know, that GRACE provides the observation of Earth's gravity field in spherical harmonic coefficients, and gravity anomaly could be obtained by subtracting the time average of gravity field from gravity field at each time epoch.

3.2 Spatial Reference Frame Unification and Time Sampling

Referring to equation (3.26) – (3.28), we obtain the monthly deformation time series. However, we are still not able to compare the deformations derived from GRACE with the displacements observed by GPS due to the inconsistency of both time and spatial reference frame. In the following we will mainly discuss the unification of the reference frame. The unification of time reference and spatial reference would be discussed respectively.

3.2.1 Center of Mass of the Solid Earth (CE)

Terrestrial reference frames are essential for modeling geodetic observations. There are several conceptually different types of reference frame used for different purposes. All the reference frames discussed in the thesis are defined as isomorphic, which indicates that the movement of the reference frames accord with the load Love number theory from Blewitt (2003).

The reference frames are related to their origins. The origins of the Earth-related frames are usually defined as one of the three centers: the center of mass of the solid Earth (CE), the center of mass of the Earth system (CM), and the center of the surface figure (CF) (Dong et al., 1997). In following, we name the frame by the name of its origin.

Firstly, the reference frame fixed to CE (CE frame) is introduced.

Theoretically, both the transfer and redistribution of the surface mass and the internal mass would influence the variation of the geocenter. The CE frame is defined at the origin of mass of the Earth without the surface mass load. Therefore, when the surface mass is redistributed, CE frame changes its trajectory in inertial space, but the position of the center of mass of the solid Earth does not change. According to this property, the CE frame is a natural frame to model the load Love numbers and to compute the dynamics of the solid Earth deformation.

However, the CE frame is not directly accessible to practical geodetic observations.

3.2.2 Center of Mass of the Earth System (CM)

The CM frame is defined on the entire Earth system, including both the solid Earth and surface mass load. CM frame is stationary with respect to the satellite orbits in inertial space. CM would remain static in inertial space, if there is no external forces on the Earth. For this case, it is an appropriate frame for modeling SLR measurements.

Since the GRACE satellite-to-satellite tracking is insensitive to degree-one mass effects, we can also consider that the measurements from GRACE are observed under the CM frame, because of the zero effect for the degree-one space potential on the satellite orbits in the CM frame.

3.2.3 Center of the Surface Figure (CF)

The CF frame is defined geometrically with origin CF, that we imagine the Earth's surface is covered by a uniform, infinitely dense array of points.

However, the CF frame could be appropriately realized by a sufficiently global dense distribution of geodetic observation stations. For this reason, it is a natural frame for GPS system.

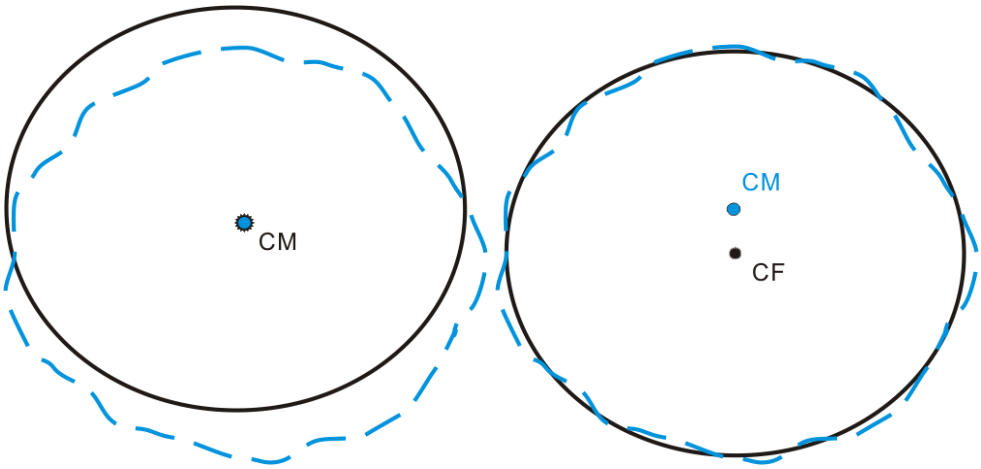

Figure 3.1: *Degree-one deformations (blue) in two different reference frame: CM (left) and CF (right)*

In figure 3.1, the relation between CM and CF is illustrated. In CM frame, the CM keeps the same in inertial space in spite of surface mass load redistribution, but mass redistribution leads to the displacement of CF. However, in CF frame, the CM is displaced before and after surface deformation.

3.2.4 Spatial Reference Frame Unification

As is described in chapter 3.2, CF frame is a natural frame for GPS, though the global GPS stations geometrically distributed and covered on the Earth do not fulfill exactly the definition that the origin of the network is at the center of the figure of the Earth.

The GRACE satellites always move around the center of mass of the Earth system, so that the GRACE observations should be given in the CM frame. However, the GRACE satellite is not sensitive to the degree-one mass effects. The coefficients of degree one represent the coordinates of the Earth's center of mass (Sneeuw, 2006). Because the measurements from GRACE are observed in the CM frame, in which the origin coincides with the center of mass, the coefficients of degree one are obtained as $C_{1,0} = C_{1,1} = S_{1,1} = 0$. Hence, GRACE is not capable to observe the terms of degree-one.

Not only the degree-one spherical harmonic coefficients but also the load Love numbers should be taken into consideration. As is noted in (Blewitt, 2003), the geocentric motion only affects

the degree-one load Love numbers while it has no influences on higher degrees. For different reference frames, the degree-one load Love numbers are not the same.

Therefore, to unify the spatial reference frame, we have two options. One is to transform the reference frame of GRACE to be consistent with the frame of GPS. The transformation can be arranged in two steps:

- Substitute the spherical harmonic degree-one coefficients for GRACE data;
- Substitute the load Love number.

The other option is to remove the degree-one terms from GPS measurements in order that the GPS and GRACE are both in CM frame.

The satellite measured global network translation relative to CM is equivalent the perturbation of degree-one coefficients (Dong et al., 1997). The translation components of the global station network solution are practically determined by Tesmer et al. (2011)

$$\begin{cases} dX = \frac{1}{n}\sum_{i=1}^{n} dX_i \\ dY = \frac{1}{n}\sum_{i=1}^{n} dY_i \\ dZ = \frac{1}{n}\sum_{i=1}^{n} dZ_i \,, \end{cases} \tag{3.29}$$

where dX_i, dY_i, dZ_i are the individual station displacements of the $i = 1, 2, 3, \ldots n$ station. Because the IGS global network is not a dense and symmetrical distribution on the globe, the terms of degree-one coefficients could not be exactly determined from GPS by network translation in equation (3.29).

The purpose of our work mainly aims at regional loading deformation analysis, e.g., Danube river basin, Tibetan Plateau, the Great Lakes, etc. So only the observations of IGS stations in those regions are included. As a result, in this thesis, we choose to substitute the degree-one coefficients obtained from (Swenson and Wahr, 2006) in GRACE data in order to convert GRACE from CM frame to CF frame.

Specified by Farrell (1972), in the CE frame degree-one load Love numbers are

$$\begin{cases} [h_1']_{\mathrm{CE}} = -0.290 \\ [l_1']_{\mathrm{CE}} = 0.113 \\ [1 + k_1']_{\mathrm{CE}} = 1 \,, \end{cases} \tag{3.30}$$

where h_1', l_1', k_1' are load Love numbers.

The translation of frame B with respect to A can be parameterized by Blewitt (2003)

$$[t_B]_A = [\alpha_B]_A \mathbf{m}/M_E \,. \tag{3.31}$$

$[t_B]_A$ is the geocenter displacement vector from frame B to A. α is the dimensionless isomorphic parameter, it depends on the conceptual definition of the reference frame origins. M_E is mass of the Earth. $\mathbf{m}$ is load moment, which is defined by (Blewitt et al., 2001)

$$\mathbf{m} = M_{\text{load}} \bar{\mathbf{r}}_{\text{load}} \,, \tag{3.32}$$

where M_{load} is mass of the surface load, $\bar{\mathbf{r}}_{\text{load}}$ is the geocenter vector of the center of mass of the load with respect to CE (Dong et al., 1997). The geocenter translates along the axis of $\mathbf{m}$.

As a result, the new degree-one load Love numbers are mathematically descirbed by Blewitt (2003) in general

$$\begin{cases} [h_1']_B = [h_1' - \alpha_B]_A \\ [l_1']_B = [l_1' - \alpha_B]_A \\ [1 + k_1']_B = [1 + k_1' - \alpha_B]_A \,. \end{cases} \tag{3.33}$$

When transferring from CE to CM, we have (Dong et al., 1997)

$$[t_{\text{CE}}]_{\text{CM}} = \frac{M_{\text{load}}}{M_E} \bar{\mathbf{r}}_{\text{load}} = \frac{\mathbf{m}}{M_E} = -[t_{\text{CM}}]_{\text{CE}} \,. \tag{3.34}$$

From equation (3.31) and (3.34), then $[\alpha_{\text{CM}}]_{\text{CE}} = 1$.

Inserting into equation (3.33), thus, the degree-one load Love numbers of CM frame with respect to CE frame can be determined by

$$\begin{cases} [h_1']_{\text{CM}} = [h_1']_{\text{CE}} - 1 \\ [l_1']_{\text{CM}} = [l_1']_{\text{CE}} - 1 \\ [1 + k_1']_{\text{CM}} = [1 + k_1']_{\text{CE}} - 1 \,, \end{cases} \tag{3.35}$$

And the $[\alpha_{\text{CF}}]_{\text{CE}}$ is derived by Blewitt (2003) through integral of total surface displacements,

$$[\alpha_{\text{CF}}]_{\text{CE}} = \frac{1}{3}[h_1' + 2l_1']_{\text{CE}} \,. \tag{3.36}$$

Inserting into equation (3.33), then the new degree-one load Love numbers of CF frame with respect to CE frame is obtained

$$\begin{cases} [h_1']_{\mathrm{CF}} = \frac{2}{3}[h_1' - l_1']_{\mathrm{CE}} \\ [l_1']_{\mathrm{CF}} = -\frac{1}{3}[h_1' - l_1']_{\mathrm{CE}} \\ [1 + k_1']_{\mathrm{CF}} = [1 - \frac{1}{3}h_1' - \frac{2}{3}l_1']_{\mathrm{CE}} \,. \end{cases} \tag{3.37}$$

As a consequence, the relations of the degree-one load Love numbers between CM frame and CF frame can finally be derived

$$\begin{cases} [h_1']_{\mathrm{CF}} = \frac{2}{3}[h_1' - l_1']_{\mathrm{CM}} \\ [l_1']_{\mathrm{CF}} = -\frac{1}{3}[h_1' - l_1']_{\mathrm{CM}} \\ [1 + k_1']_{\mathrm{CF}} = [-\frac{1}{3}h_1' - \frac{2}{3}l_1']_{\mathrm{CM}} \,. \end{cases} \tag{3.38}$$

What we need to do in the next step is to substitute the degree-one load Love numbers in CM frame by those in CF frame. Both GRACE and GPS are then in the equivalent spatial reference frame.

3.2.5 Time Sampling

Different from spatial reference frame unification, we need to unify the time reference frame in case of the incompatible temporal resolutions. The observations from GPS are weekly while solutions provided by GRACE are once a month. For this reason, it is indispensable to unify the temporal resolutions. To avoid time aliasing and inaccurate interpolation, we choose to average the GPS weekly observations over one month and choose the time epoch to be at the middle of each month. For example, if the deformations of four epochs are observed in May, then we obtain the average of those four deformations as one monthly deformation, and make the time epoch be on May 15th. For daily solutions, we just make an average of thirty days, and also choose the time epoch to be at the middle of each month.

Then we choose the same time period of long-term observations for GPS and GRACE. As a result, the synchronized time series from GPS and GRACE are obtained.

3.3 Filtering

Since the signal usually contains noise, to acquire useful information and reduce the noise from the original signal, the signal need to be filtered. Because of the noises contained in GRACE signal, several different types of filters are designed for GRACE data smoothing, such as Gaussian isotropic (Jekeli, 1981; Wahr et al., 1998; Devaraju and Sneeuw, 2012) and non-isotropic smoothing (Han et al., 2005; Kusche, 2007; Guo et al., 2010), destriping filter (Swenson and Wahr, 2006), and stochastic filter (Sasgen et al., 2006; Klees et al., 2008).

3.3.1 Gaussian Filter

The Gaussian filter is a deterministic filter. It does not depend on the real signal but on the mathematical analysis of models. For the Gaussian filter, the weight function in the spatial domain is (Jekeli, 1981)

$$W = e^{-r(1-\cos\alpha)}, r > 0\,, \tag{3.39}$$

where W is the weight in spatial domain, α is the spherical distance on the sphere, and r is the averaging radius.

Developed by Wahr et al. (1998), we use the averaging normalized function in spatial domain here so that

$$W(\alpha) = \frac{b}{2\pi} \cdot \frac{e^{-b(1-\cos\alpha)}}{1-e^{-2b}} \tag{3.40}$$

$$b = \frac{\ln(2)}{1-\cos(r/R)}\,, \tag{3.41}$$

Where r is regarded as the averaging radius, R is the Earth's mean radius, $W(\alpha)$ is a function of spherical distance α on the Earth's surface.

Because of the relationship

$$W_l = \int_0^{\pi} W(\alpha) P_l(\cos\alpha)\sin\alpha d\alpha\,, \tag{3.42}$$

where

$$P_l = \frac{\bar{P}_{l,m=0}}{\sqrt{2l+1}}$$

are the Legendre polynomials.

Thus, instead of in spatial domain $W(\alpha)$, we can finally get the Gaussian averaging function W_l in spectral domain for filtering spherical harmonic coefficients which depends only on degree l.

To make the computation efficient and convenient, the Gaussian averaging function in spectral domain is formulated recursively by Wahr et al. (1998):

$$W_0 = \frac{1}{2\pi} \tag{3.43}$$

$$W_1 = \frac{1}{2\pi}\left[\frac{1+e^{-2b}}{1-e^{-2b}} - \frac{1}{b}\right] \tag{3.44}$$

$$W_{l+1} = -\frac{2l+1}{b} \cdot W_l + W_{l-1} \,. \tag{3.45}$$

The Gaussian filter is very important and will be used later in smoothing of GRACE data. It is an isotropic averaging filter, which means that the function W_l only depends on degree l.

The spherical harmonic spectrum of a non-isotropic averaging function is given by Han et al. (2005)

$$W_{lm} = W_l(r_{1/2}(m)) \tag{3.46}$$

$$r_{1/2}(m) = \frac{r_1 - r_0}{m_1} \cdot m + r_0 \,, \tag{3.47}$$

where $r_{1/2}$ are the averaging radii, m is the averaging order. The spatial resolution of non-isotropic smoothing is determined by r_0 in latitude and by r_1 and m_1 in longitude direction.

Unlike the isotropic smoothing, W_{lm} depends both on degree and order. Leading to a non-isotropic shape consequently in spatial domain, the W_{lm} is called anisotropic Gaussian smoothing. When the $r_0 = r_1$, the W_{lm} turn to be the isotropic Gaussian averaging function W_l again with averaging radius r_1 as a special case.

Different from isotropic smoothing, anisotropic filter can effectively pass the higher degree and lower order coefficients while reject undesired higher order coefficients. For this reason, anisotropic Gaussian filter might be more appropriate for GRACE data smoothing, and this will discussed in detail and compared with isotropic Gaussian filter in chapter 4.5.

3.3.2 Destriping Filter

Because of the correlated error in the spectral domain, the destriping filter is also called correlated-error filter, which is proposed by Swenson and Wahr (2006).

The correlated-error filter is aim to remove the spatial correlated errors that presented in GRACE data. Swenson and Wahr (2006) found that there is no apparent correlations between even and odd coefficients, however, the correlated behaviors appear at approximately $m = 8$ and also in higher orders. The destriping filter can be described by

$$\Lambda_{lnm} = \sum_{i=0}^{p} \sum_{j=0}^{p} L_{ij}^{-1} n^i l^i \,, \tag{3.48}$$

which leads to the smoothed spherical harmonic coefficients C_{lm}^{ce} expressed as

$$C_{lm}^{\mathrm{ce}} = \sum_{n=l-\frac{w}{2}}^{l+\frac{w}{2}} \Lambda_{lnm} C_{nm}, \; n : \text{even or odd} \,, \tag{3.49}$$

where

$$L_{ij} = \sum_{n=l-\frac{w}{2}}^{l+\frac{w}{2}} n^i n^j, \; n : even\ or\ odd\ , \tag{3.50}$$

and n denotes the degree that includes only the same parity as degree l.

In this case, the spherical harmonic coefficients are smoothed for a particular order m with a quadratic polynomial in a moving window centered about degree l, where p is the order of the polynomial, w is the width of the smoothing window. More details can be seen in (Swenson and Wahr, 2006).

Hence, in the thesis, the combination of destriping filter and Gaussian averaging filter will be tested in order to find out the optimal choice of filtering for GRACE data.

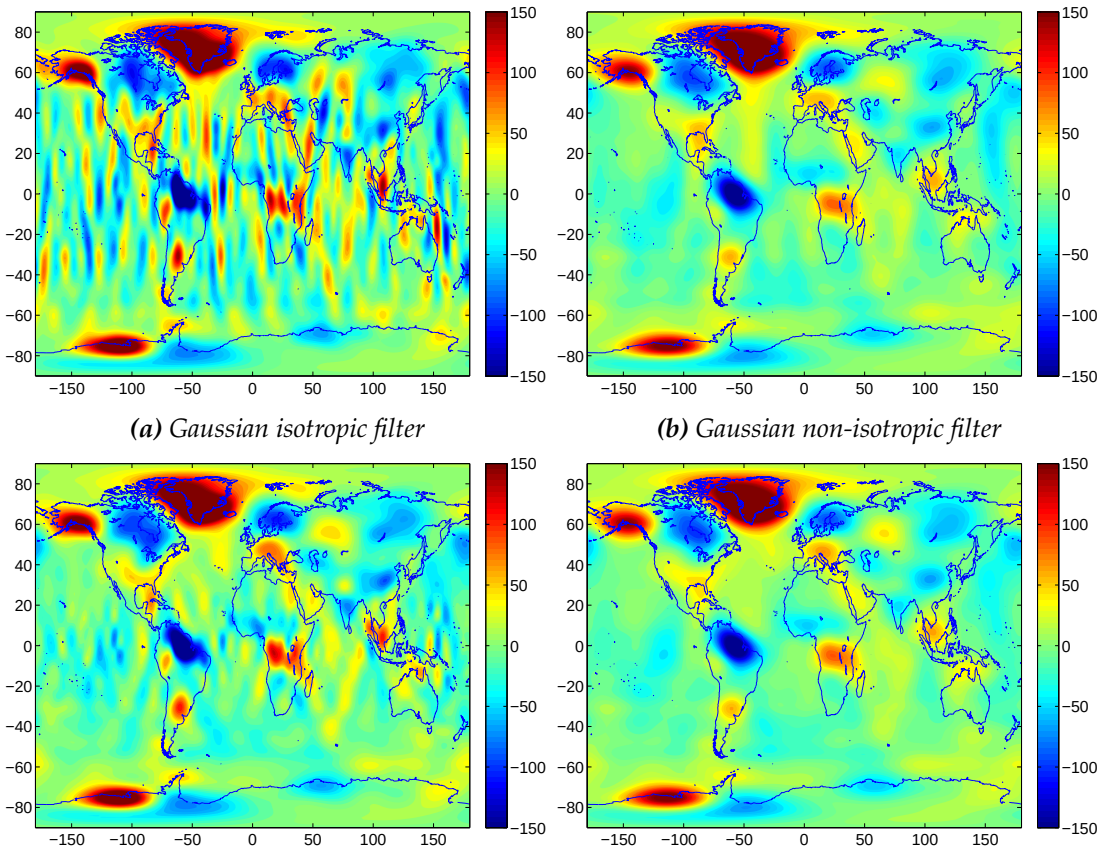

(a) *Gaussian isotropic filter*

(b) *Gaussian non-isotropic filter*

(c) *Destriping filter + Gaussian isotropic*

(d) *Destriping filter + Gaussian non-isotropic*

Figure 3.2: *GRACE equivalent water height (EWH) after filtering with different filters*

3.3.3 Stochastic Filter

In contrast to the deterministic filter, which only depends on an averaging radius, stochastic filters are operators that take the errors of the signal into account. Therefore, stochastic filters designed for the spherical harmonic coefficients are proposed by Sasgen et al. (2006).

A stochastic filter can deliver an optimum estimate either by maximizing the signal-noise ratio or by minimizing the variance of the overall estimation error. The Wiener filter is belong to the latter.

The observed signal $x(\theta, \lambda)$ is composed of

$$x(\theta, \lambda) = y(\theta, \lambda) + n(\theta, \lambda) \,, \tag{3.51}$$

where $n(\theta, \lambda)$ is the noise on the desired signal $y(\theta, \lambda)$. The task of the filter is to eliminate or reduce this noise.

The filtered signal $\hat{x}(\theta, \lambda)$ can be expressed by spatial convolution of the filter response function H with observed signal $x(\theta, \lambda)$,

$$\hat{x}(\theta, \lambda) = H * x(\theta, \lambda) \,, \tag{3.52}$$

then

$$\varepsilon = \hat{x}(\theta, \lambda) - x(\theta, \lambda) \,, \tag{3.53}$$

where H is the impulse response of the Wiener filter, $*$ notation means convolution operator, and ε is the estimation error.

The Wiener filter aims to minimize the target function based on Least-Squares method:

$$\sigma^2 = E[\{\varepsilon\}^2] = \min \,, \tag{3.54}$$

where E is the expectation operator.

The signal $x(\theta, \lambda)$ and $y(\theta, \lambda)$ can be represented respectively in form of scalar spherical harmonics $Y_{lm}(\theta, \lambda)$ defined in equation (3.3) with spherical harmonic expansion coefficients x_{lm} and y_{lm} of degree l and order m (Sasgen et al., 2006) as

$$x(\theta, \lambda) = \sum_{l=0}^{\infty} \sum_{m=0}^{l} x_{lm} Y_{lm}(\theta, \lambda) \tag{3.55}$$

$$y(\theta,\lambda) = \sum_{l=0}^{\infty}\sum_{m=0}^{l} y_{lm} Y_{lm}(\theta,\lambda)\ . \tag{3.56}$$

Here, the spherical harmonic coefficients a_{lm} and b_{lm} defined in equation (3.7) are contained in both the observed coefficients x_{lm} and filtered coefficients y_{lm}.

So that

$$x_{lm} = y_{lm} + n_{lm}\ , \tag{3.57}$$

where n_{lm} is the noise of coefficients in spectral domain.

And the spatial convolution in form of spherical harmonics are reformulated,

$$\sum_{l=0}^{\infty}\sum_{m=0}^{l} \hat{x}_{lm} = \sum_{l=0}^{\infty}\sum_{m=0}^{l} h_l x_{lm}\ . \tag{3.58}$$

Notice that the Wiener filter adopted in this thesis is isotropic and therefore the filter kernel h_l is dependent only on the degree l of the signal and noise

According to the Least-Squares method, the minimum mean square error (MMSE) σ^2 should meet the requirement,

$$\sigma^2 = E\left[\sum_{l=0}^{\infty}\sum_{m=0}^{l} (y_{lm} - \hat{x}_{lm})^2\right] = \min\ . \tag{3.59}$$

Then

$$\frac{\partial \sigma^2}{\partial h_l} = 0\ , \tag{3.60}$$

which finally leads to the kernel of the Wiener filter

$$h_l = \frac{\sigma^2_{y,l}}{\sigma^2_{y,l} + \sigma^2_{n,l}}\ , \tag{3.61}$$

where $\sigma^2_{y,l}$ is the degree variance of desired signal and $\sigma^2_{n,l}$ is the degree variance of error.

The Wiener filter requires prior knowledge of the desired signal when it is implemented. However, such prior information does not exist in the case of GRACE spherical harmonic coefficients. Thus, $\sigma^2_{y,l}$ is unknown. Due to this reason, it is essential to determine the a priori variance of signal. One can determine the a priori variance through geophysical model. Lorenz (2009) solved this problem by a simulation for a full covariance matrix of time-variable GRACE coefficients. This simulated full covariance matrix is adopted for the Wiener filtering in the thesis, and the filtered GRACE coefficients are then provided by Mr. Devaraju [1].

[1] Institute of Geodesy, University of Stuttgart (balaji.devaraju@gis.uni-stuttgart.de)

3.4 Correction for Atmosphere and Ocean Effects

For both GRACE and GPS, the effects of the solid Earth tides, ocean tides and pole tides were already subtracted. The GSM product used in the thesis for GRACE deformation derivation contains only the estimate of the static gravity field from GRACE observations (Bettadpur, 2007). That is to say, the tidal and non-tidal atmospheric and oceanic effects have been already accounted and removed in GSM product. However, the deformations observed by GPS still contain the influences from atmosphere and ocean. Thus, it is necessary to correct the effects of atmosphere and oceans for both GPS and GRACE.

Consequently, one can either remove those effects from GPS to be in accordance with GRACE, or add the non-tidal atmospheric and barotropic ocean mass fields back to the estimated fields from GRACE in order to be consistent with GPS measurements.

The deformations influenced by atmosphere and ocean loading could not be separately calculated, so those effects could be hardly removed from GPS time series.

The non-tidal atmospheric and oceanic mass field variation models are generated by GFZ in GRACE Atmosphere and Ocean De-aliasing Level-1B (AOD1B) products, and the spherical harmonic coefficients of the non-tidal atmosphere and ocean are included as a combination estimate in GRACE GAC product. So the loading effects of the ocean and atmosphere could be determined using the AOD1B data (Flechtner and Potsdam, 2007). Hence, it would be better and more convenient to add the corrections back to the static gravity field estimate from GSM product when deriving the surface displacements.

In conclusion, the whole procedure of data processing could be graphically described in figure 3.3.

3.5 Statistical Measures

When comparing the deformation time series between GPS and GRACE, we have to quantitatively evaluate the disagreement between two observation techniques by statistical methods.

3.5.1 Correlation

To evaluate how much similarity between two time series, at first the correlation coefficient is introduced. The correlation R between the time series from GPS and GRACE can in practice be calculated by

$$R = \frac{\frac{1}{N}\sum_{n=1}^{N}(\mathrm{GPS}_n - \overline{\mathrm{GPS}})(\mathrm{GRACE}_n - \overline{\mathrm{GRACE}})}{\sigma_{\mathrm{GPS}}\sigma_{\mathrm{GRACE}}}, \tag{3.62}$$

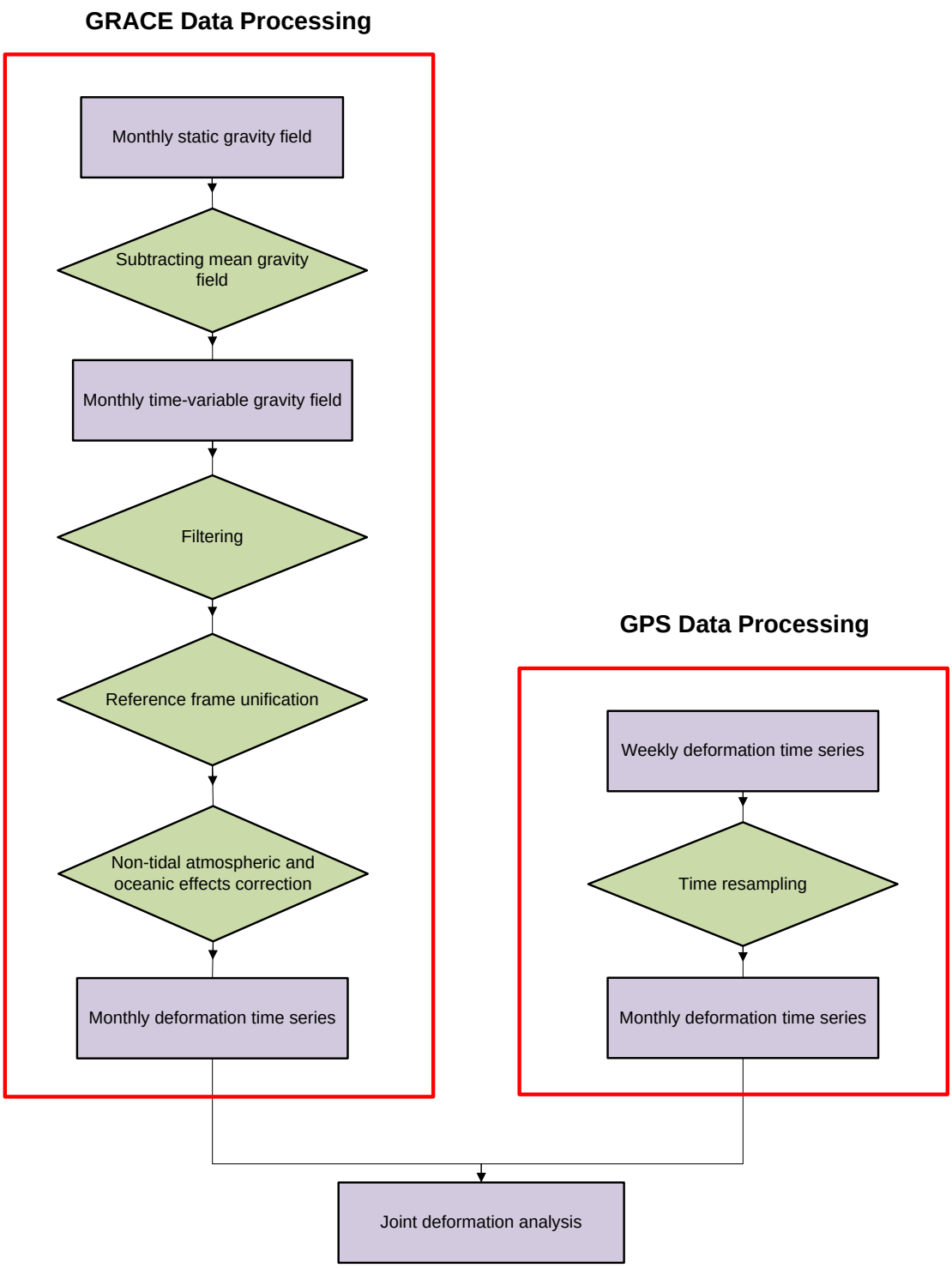

Figure 3.3: *Data processing chain*

where σ_{GPS}, σ_{GRACE} are respectively the variance of time series of GPS and GRACE, $\overline{\text{GPS}}$, $\overline{\text{GRACE}}$ and are the mean values of two time series.

In general, the correlation coefficients quantitatively describe the similarity between two different time series. However, it could only reflect the similarity in phase but ignore the difference in amplitude. For instance, two time series have the identical phases but completely different amplitudes. So the correlation coefficient with value 1 shows perfectly correlation between two time series even though there is great discrepancy of amplitudes.

3.5.2 Nash-Sutcliffe Efficiency

Another important index which can reflect the similarity between two time series is the Nash-Sutcliffe Model Efficiency Coefficient or Nash-Sutcliffe Efficiency (NSE) for short. NSE is commonly used to assess the predictive power of, e.g., a hydrological model. In this thesis, it is applied to quantitatively evaluate the amplitude discrepancy between GPS and GRACE. Here we regard the GRACE time series as model.

NSE is a normalized statistic that determines the relative the magnitude of the residual variance compared to the measured data variance (Moriasi et al., 2007). NSE indicates how well the observed data fits the simulated data. It is defined as (Nash and Sutcliffe, 1970):

$$\text{NSE} = 1 - \frac{\sum_{n=1}^{N}(\text{GPS}_n - \text{GRACE}_n)^2}{\sum_{n=1}^{N}(\text{GPS}_n - \overline{\text{GPS}})^2} \tag{3.63}$$

where Y_n^{GPS} is the observed data, GRACE_n is the modeled data, and $\overline{\text{GPS}}$ is the mean of GPS.

NSE can range from $-\infty$ to 1. When $\text{NSE} = 1$, it means that the GRACE and GPS signals have perfect consistency. An efficiency of 0 $(\text{NSE} = 0)$ indicates that GRACE is equivalent with the mean of GPS. NSE values between 0 and 1 $(0 < \text{NSE} < 1)$ generally indicates that the mean GPS signal fits quite well with the GRACE signal, so it could be viewed as acceptable level of amplitude discrepancy from GPS and GRACE. Whereas the NSE value is less than 0 $(\text{NSE} < 0)$, it indicates great discrepancy of amplitudes between GPS and GRACE signals. That is to say, it is an unacceptable level.

In summary, the closer the NSE value is to 1, the better GPS and GRACE agree. When we analyze the performance of GPS and GRACE, both correlation coefficient and NSE should be taken into account for evaluation.

3.5.3 WRMS Reduction

A further quality measure would be the question how well the GRACE and GPS signals agree by comparing the weighted root mean square (WRMS) of the GPS signal before and after removing the GRACE signal.

Here, the WRMS of GPS signal is given by the formula

$$\mathrm{WRMS(GPS)} = \sqrt{\frac{1}{N}\sum_{n=1}^{N} W_n \cdot \mathrm{GPS}_n^2}\,, \tag{3.64}$$

where the GPS_n denotes GPS observation at each epoch, and the W_n is the weight value, which can be determined by the standard deviation σ_{GPS} of each epoch

$$W_n = \frac{1}{\sigma_{\mathrm{GPS},n}^2}\,. \tag{3.65}$$

After removing GRACE from GPS signal, the WRMS turns to be

$$\mathrm{WRMS(GPS-GRACE)} = \sqrt{\frac{1}{N}\sum_{n=1}^{N} W_n \cdot (\mathrm{GPS}_n - \mathrm{GRACE}_n)^2}\,, \tag{3.66}$$

in which the GRACE_n is GRACE observation at each epoch, and W_n' turns to be the weight value of both GPS and GRACE observations. According to the error propagation, then

$$W_n' = \frac{1}{\sigma_{\mathrm{GPS},n}^2 + \sigma_{\mathrm{GRACE},n}^2} \tag{3.67}$$

in terms of standard deviations σ_{GPS} from GPS and σ_{GRACE} from GRACE. To get the standard deviation σ_{GRACE}, we need also to filter the Stokes coefficients of errors and calculate the σ_{GRACE} in spatial domain from spectrum domain through error propagation principle. In this thesis, to make it simple, the weight matrix W_n' of GPS signal after removing GRACE is regarded the same as W_n in equation (3.65).

The reduction of the GPS signal WRMS by subtracting GRACE signal from GPS is proposed by (van Dam et al., 2007)

$$\mathrm{Reduction} = \mathrm{WRMS(GPS)} - \mathrm{WRMS(GPS-GRACE)}\,, \tag{3.68}$$

which could also be represented relatively as

$$100 \cdot \left(\frac{\text{WRMS(GPS)} - \text{WRMS(GPS} - \text{GRACE)}}{\text{WRMS(GPS)}} \right) , \tag{3.69}$$

where WRMS(GPS) is the WRMS of the GPS signal, WRMS(GPS-GRACE) is the WRMS of the residuals between GPS and GRACE signals.

We can say that, the larger the WRMS reduction is, the better GPS accords with GRACE. Whereas the WRMS reduction is less than 0, the WRMS of the GPS signal get even worse than the one before removing GRACE from GPS, which indicates that GPS time series behaves completely different from GRACE time series.

Combining equation (3.64), (3.66) and (3.68), then

$$\text{Reduction} = 1 - \sqrt{\frac{1}{N} \sum_{n=1}^{N} \frac{W'_n \cdot (\text{GPS}_n - \text{GRACE}_n)^2}{W_n \cdot \text{GPS}_n^2}} \tag{3.70}$$

Comparing equation (3.63) with (3.70), we find that NSE is implicitly correlated with WRMS reduction in mathematical aspect. That is to say, even though NSE and WRMS reduction are computed in two different ways, they indicate the same conclusion. NSE is widely used for hydrological analysis, and WRMS reduction is a major indicator of evaluating the similarity between GPS and GRACE time series in many journal articles. Therefore, both of them are adopted in this thesis so that the results could be easily compared with the work of other researchers.

3.5.4 Least Squares Fitting

In earth system, most of phenomena happened annually. However, because of the measurement errors such as the noises, the observed signal usually has not exactly annual pattern. Therefore, in order to show the regularity and analyze the observations from geodetic techniques, it requires us to fit an annual mean signal to the observed signal.

Generally, the annual signal can be fitted by the mathematical model:

$$y_i = A \sin \left[\omega (t_i - t_0) + \phi \right] , \tag{3.71}$$

where A is the amplitude and ϕ is the phase, ω is the frequency of signal, t_i is the observation epoch and t_0 is the first epoch, y_i represents the annual signal. Here because of its annual pattern, the ω is defined as 2π.

In fact, the observations are not rigorous annual signal. Thus, the Gauss-Markov model can be applied for those observations, and in avoid of linearization then they are expressed as:

$$y_i = A_1 \sin(\omega \Delta t_i) + A_2 \cos(\omega \Delta t_i) \ , \tag{3.72}$$

where

$$\Delta t_i = t_i - t_0 \ .$$

So far, the Least-Squares adjustment could be applied to solve the unknown A_1 and A_2 by

$$N = [\sin(\omega \cdot dt), \cos(\omega \cdot dt)] \tag{3.73}$$

$$[\hat{A}_1 \ \hat{A}_2]^T = (N^T N)^{-1} N^T y \ . \tag{3.74}$$

To solve the unknown annual amplitude A and phase ϕ, the equation 3.71 and 3.72 are combined, so the solutions read:

$$\hat{A} = \sqrt{\hat{A}_1^2 + \hat{A}_2^2} \tag{3.75}$$

$$\hat{\phi} = \arctan\left(\frac{\hat{A}_2}{\hat{A}_1}\right) \ . \tag{3.76}$$

And the mean annual fitted signal $\hat{y}$ is finally obtained by

$$\hat{y} = \hat{A} \sin\left[\omega(t_i - t_0) + \hat{\phi}\right] \ . \tag{3.77}$$

Chapter 4

Data Analysis

4.1 Datasets

The IGS stations globally distribute on the Earth, which observe the GPS satellites and then provide long-term position time series of IGS stations by GPS observations. While, the spherical harmonic approach is essentially applied globally for Earth's gravity field analysis.

However, our objective focuses mainly on regional study. In order to achieve the objective of this thesis, we analyze the deformation time series from GPS and GRACE separately in three selected different areas, including Danube area in Europe, Tibetan plateau in Asia and the Great Lakes area in North America. So they can typically represent the load variations happened on the Earth.

The GRACE data we used in the thesis are Release-05 monthly solutions, coming from GFZ with time period of 9 years (2003.01-2012.09). Considering that GRACE does not recover $l = 1$ terms (see chapter 3.2.4) and the $C_{2,0}$ coefficients have anomalously large variability, the degree-one coefficients are gained from Swenson [1], and $C_{2,0}$ coefficients are replaced already from GFZ product (Dahle et al., 2012). The GPS data processing is done and weekly deformation time series of IGS stations are provided by China and IGN in France. To keep a equivalent time reference, the monthly deformation time series are averaged from GPS weekly data afterwards

[1] Department of Physics and Cooperative Institute for Research in Environmental Sciences (CIRES), University of Colorado, Boulder, Colorado, USA

Table 4.1: *Datasets description*

GRACE data	GFZ Release 05 (2003.1-2012.9)
GPS data (weekly)	Xavier Collilieux
GPS data (daily)	Dr.Rong Zou with GIPSY/OASIS II 5.0
Degree-1 coefficients	Swenson et.al (2008)
$C_{2,0}$ coefficients	SLR

Table 4.2: Parameters of filter schemes

Gaussian anisotropic filter	m_1 = 15 r_0 = 500 km r_1 = 1000 km
Destriping filter	l: 8∼90 m: 8∼90 polynomial order: 2

(described in chapter 3.2.5). The detailed datasets and relevant parameters are listed in table 4.1.

Before derivation of the deformation time series from GRACE, the filtering is necessary for GRACE signal. In this thesis, we mainly choose the Gaussian anisotropic filter with radius of 500 km and combine with destriping filter for data pre-processing. And the detailed parameters for filters are shown above in the table 4.2.

Considering that deformation time series observed by GPS contain random noises, the GPS monthly time series have to be smoothed in a certain scale before compared with GRACE. In case of noisy expression, five-month mean is preferred. To keep consistency, the GRACE monthly time series would be smoothed in five-month scale as well.

4.2 Tibetan Plateau

Due to the limited time period of observations, only 5 IGS stations located on Tibetan plateau are provided by Dr. Rong Zou and then will be analyzed. And the locations of these stations are shown as below:

4.2.1 Vertical Deformation Time Series Comparisons

The vertical deformation time series are derived from GRACE spherical harmonic coefficient changes (by equation (3.26)), and the deformation time series from GPS have already been processed by Dr. Rong Zou [2]. Thus, what we need to do is to synchronize both two kinds of time series in a equivalent reference frame (described in chapter 3.2.4).

For comparisons, we evaluate the disagreements between GRACE and GPS by three different statistical terms: correlation coefficient, weight mean root square (WRMS) reduction, Nash-Sutcliffe coefficient. And those coefficients are listed in table 4.3.

[2]Institute of Geophysics and Geomatics, China University of Geosciences, No.388 Lumo Road, Wuhan, Hubei, 430074, P.R.China

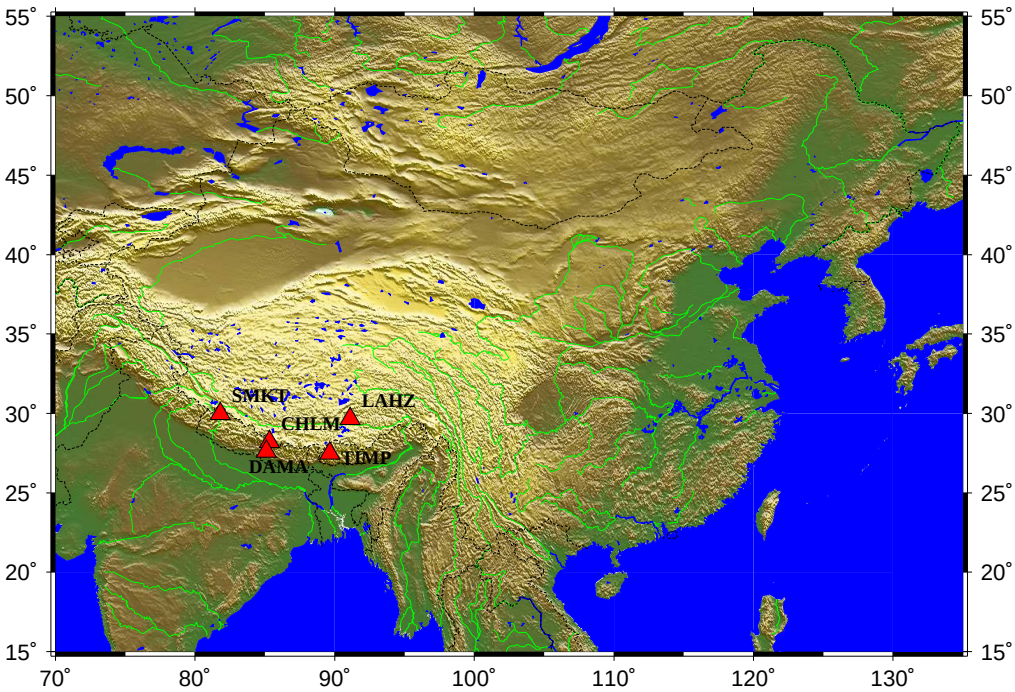

Figure 4.1: *IGS Stations on Tibetan Plateau*

Table 4.3: *Vertical deformation comparisons in terms of statistical coefficients*

Station	Correlation Coefficient	WRMS Reduction (%)	Nash-Sutcliffe Coefficient
CHLM	0.88	51.2	0.76
DAMA	0.93	61.9	0.84
LHAZ	0.65	14.8	0.24
SMKT	0.97	11.6	-0.02
TIMP	0.83	41.6	0.67

From table 4.3, the correlation coefficients of all five stations show quite high correlations, which are all above 0.5, while the WRMS reductions do not have the consistent performance as correlation even though all of them have positive reductions. As we know, only the correlation coefficients is not capable to reflect exactly the real performance due to that it is not sensitive to the discrepancy of amplitudes. From Nash-Sutcliffe efficiency (NSE) coefficients, only SMKT station has negative values while all the other four stations have positive values, which can reveal that the vertical deformations of SMKT from GRACE and GPS have big difference in amplitude. The amplitude discrepancy could be obviously seen in figure 4.3.

Above all, it can be concluded that the deformations of all five stations from GRACE and GPS are highly correlated but without consistent amplitudes.

In figure 4.2, all the five stations show roughly annual behaviors. the deformation time series from GRACE and GPS have to be smoothed in five-month scale before compared in case of noisy expression.

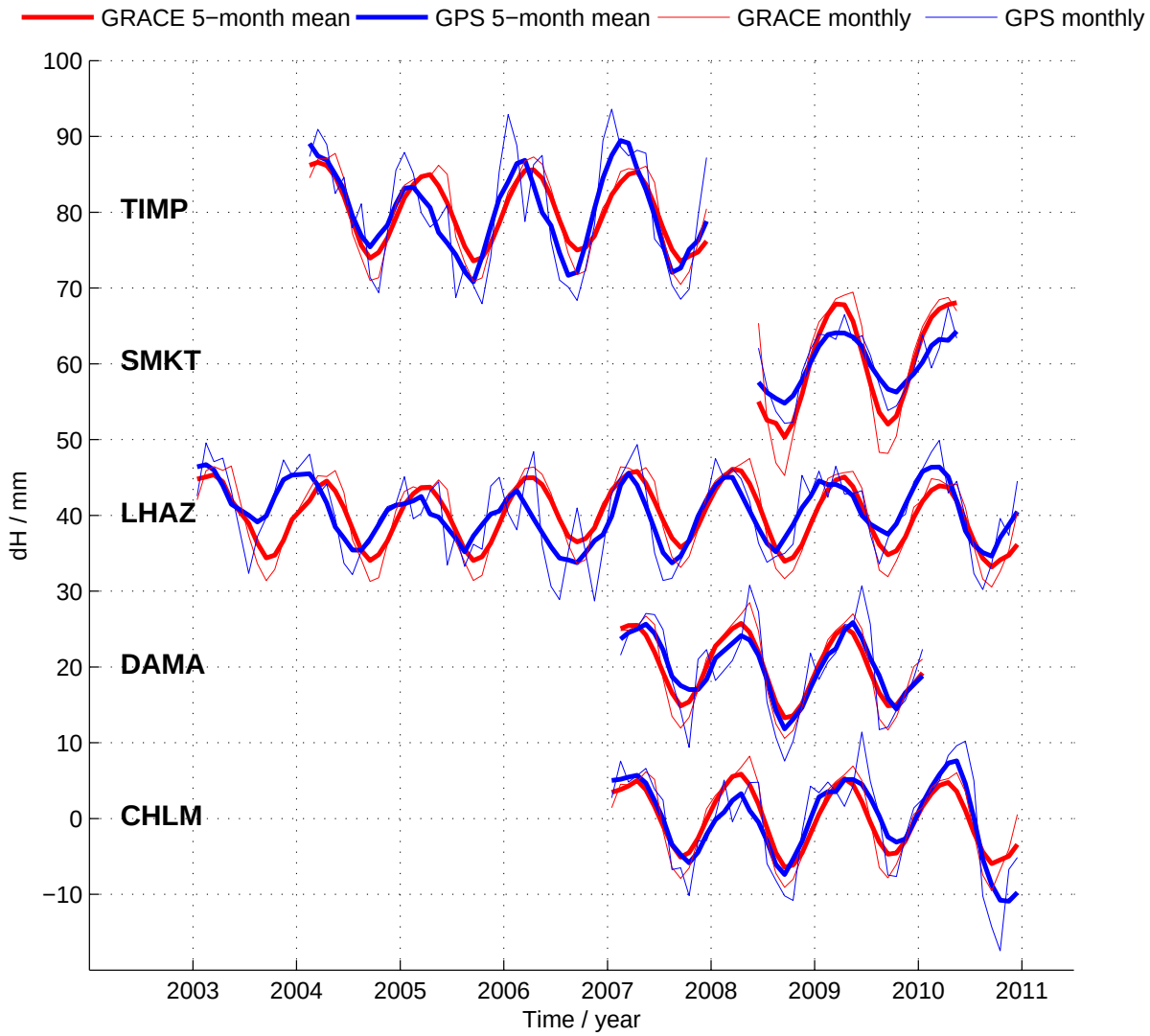

Figure 4.2: *Comparisons of height deformation time series from GRACE and GPS on Tibetan plateau*

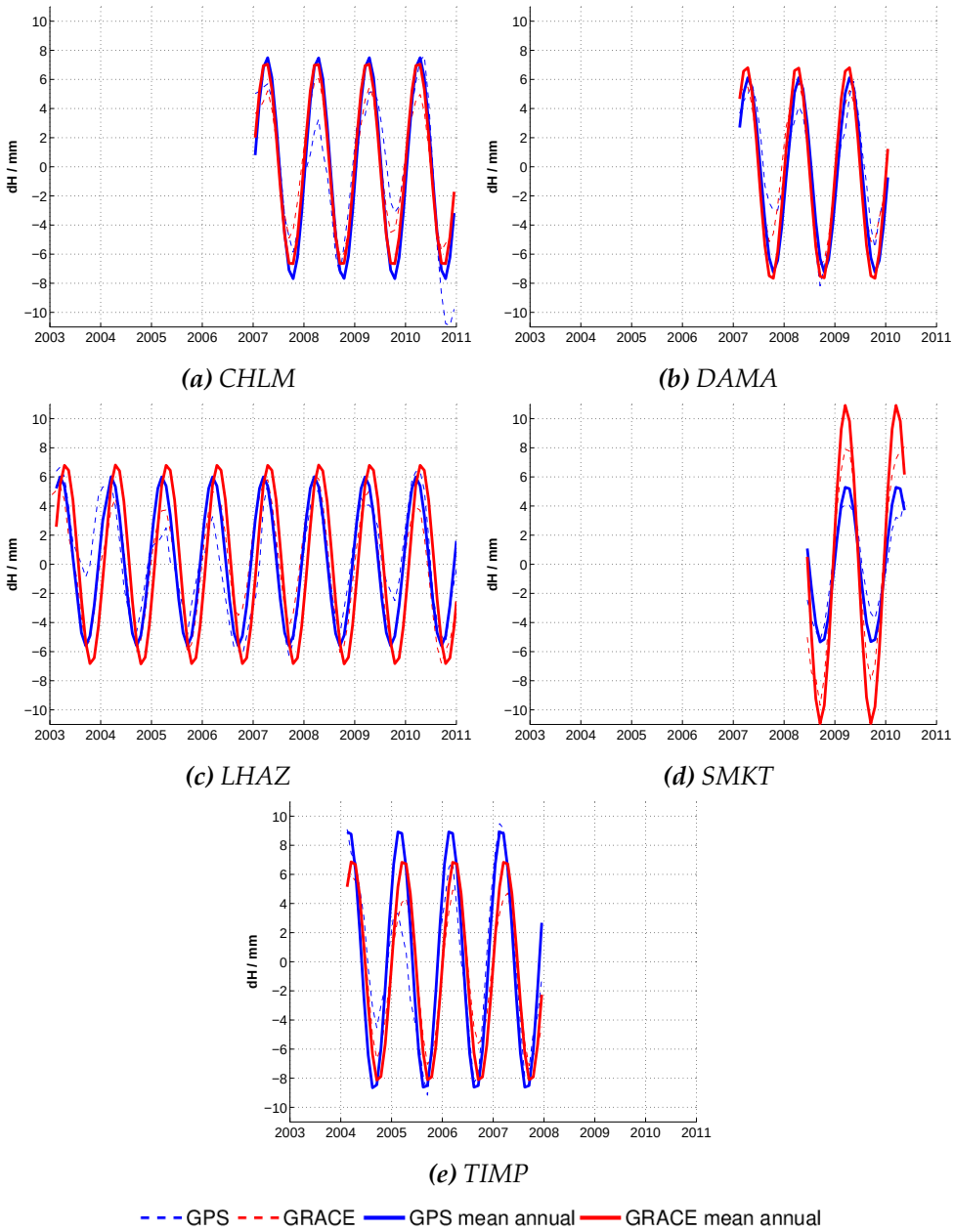

Figure 4.3: *Annual mean height deformation time series of from GRACE and GPS on Tibetan plateau*

In order to know how the deformations act averagely in every year, the mean annual deformation time series shown in figure 4.3 are then calculated to fit the original signals. In figure 4.3, LHAZ shows slight phase shift so that the deformations from GRACE are not perfectly correlated with deformations from GPS, and SMKT shows that there is a large discrepancy between GPS and GRACE. In other word, it can illustrate the negative NSE values.

Combining the figure 4.2, 4.3, and table 4.3, it is proved that the CHLM station has very high correlation, large WRMS reduction after removing GRACE, and quite slight amplitude discrepancy. It shows higher consistency than other four stations on Tibetan plateau.

4.2.2 Disagreement Analysis between GRACE and GPS

In chapter 4.2.1, only the vertical deformation time series on Tibetan plateau are analyzed. In fact, Tibetan plateau is an extremely complicated area, in which the surface displacements are influenced by numbers of factors, not only by hydrological loading variation but also by tectonic motions. Hence, the deformations in horizontal direction would not be compared and analyzed here.

To evaluate the relevancy of vertical deformation of five stations on Tibetan plateau, the monthly deformations of all the five stations are visualized together in figure 4.2.

In this figure, the common annual patterns of five stations can be seen obviously, that the deformations rise up from winter and fall down in summer. As the periodical deformations may due to surface load variation, it might be described that the surface load becomes larger in summer and then gradually removed from winter. That reveals all the five stations are strongly influenced by seasonal loading variation, and the seasonal loading variation can be regarded mainly from hydrological signal. On the other hand, it may be concluded that radial deformations are supposed to distinctly reflect the surface loading variation on Tibetan plateau.

4.3 Danube Area

In this part, 15 IGS stations located around the Danube river basin will be analyzed. And the locations of these stations are shown as below in figure 4.4.

4.3.1 Vertical Deformation Time Series Comparisons

Since the weekly deformation time series from GPS are provided by Xavier Collilieux [3], the left work is to derive the vertical deformation time series from GRACE spherical harmonic coef-

[3] French National Institute of geographic and forest information (IGN), France

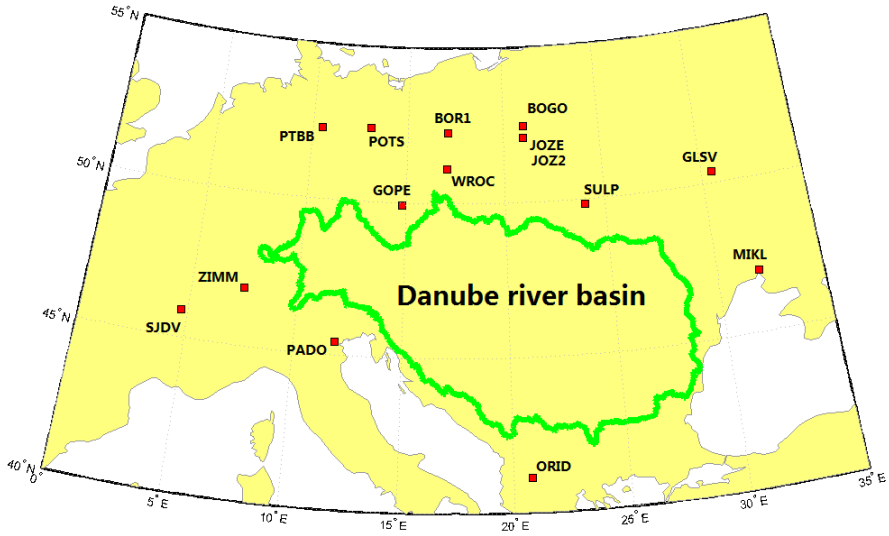

Figure 4.4: *IGS Stations in Danube Area*

ficient changes (by equation (3.26)). Besides that, according to chapter 3.2.4, the deformation time series from GRACE and GPS are synchronized in a same reference frame.

To compare the deformations from GRACE and GPS, we evaluated the disagreements between two geodetic observation techniques by means of correlation coefficient, WRMS reduction, and NSE coefficient. And the statistical information can be found in table 4.4.

Table 4.4: *Vertical deformation comparisons in terms of statistical coefficients*

Station	Correlation Coefficient	WRMS Reduction (%)	Nash-Sutcliffe Coefficient
BOGO	0.83	43.5	0.67
BOR1	0.85	45.9	0.71
GLSV	0.86	45.2	0.70
GOPE	0.66	24.3	0.42
JOZ2	0.73	30.6	0.51
JOZE	0.71	29.6	0.50
MIKL	0.93	61.0	0.85
ORID	0.82	32.4	0.53
PADO	0.81	38.3	0.62
POTS	0.79	32.7	0.54
PTBB	0.55	7.4	0.13
SJDV	0.24	-7.2	-0.17
SULP	0.90	51.9	0.77
WROC	0.54	15.7	0.27
ZIMM	0.39	2.8	0.05

From table 4.4, except for SJDV and ZIMM stations, the correlation coefficients of other 13 stations show quite high correlations, which are above 0.5, while the WRMS reductions have not the consistent performance as correlations.

Three of these stations have less than 20 percent WRMS reduction, even the SJDV has negative reduction after removing GRACE from GPS observations, which indicates the deformations derived from GRACE are mostly opposite to the deformations observed by GPS.

Depending only on the correlation coefficients, it is not sufficient that cannot reflect actually the discrepancy of amplitudes. Thus, from NSE coefficients, all the stations except for SJDV have positive values, which can reveal that the vertical deformations of SJDV from GRACE and GPS have big difference in amplitude. Later in section 4.3.3, the detailed analysis of vertical deformations of some representative stations will be discussed.

To sum up, the vertical deformations in Danube area mostly show high correlations so that deformations from GRACE behave quite similar to GPS.

In figure 4.5, monthly deformations of eight stations are shown. All of the eight station shown in this figure have roughly annual behaviors. The time series of GPS and GRACE have already been both smoothed in five-month scale (as in chapter 4.2.1). The mean annual deformation time series are shown in figure 4.6 that can indicate the average deformations in every year, which are estimated from the 8-year monthly time series. From this figure, mean annual deformations from GRACE fit very well with ones from GPS though still amplitude discrepancy existed.

To compare the annual amplitudes in vertical direction from GRACE and GPS, we plot the mean annual amplitudes from all 15 stations in figure 4.7, and a line fit to the amplitudes from those stations in order to visually see the amplitude discrepancy. Only if all the GPS annual signals have completely same amplitudes, then the slope of the best fit line would be 1. Therefore, it can be concluded that mostly deformations from GPS have lager amplitudes than from GRACE, which indicates that not all the deformations contained in GPS signal are induced by the surface water load variations.

4.3.2 Horizontal Deformation Time Series Comparisons

Like the vertical deformation derivation, the deformations in horizontal direction would be derived from the GRACE spherical harmonic coefficient changes by equation (3.27) – (3.28), and the spatial and temporal reference are unified.

The disagreements between GRACE and GPS are evaluated as well by correlation coefficient, WRMS reduction, and NSE coefficient. And the results are listed in table 4.5 and 4.6.

From table 4.5 and 4.6, comparing with vertical deformations, nearly all the stations show very low even negative correlations, which indicates that in horizontal direction deformations from GRACE and GPS are not well correlated. The situation in east seems to be a little bit better than in north, that only three stations show positive correlation in north direction.

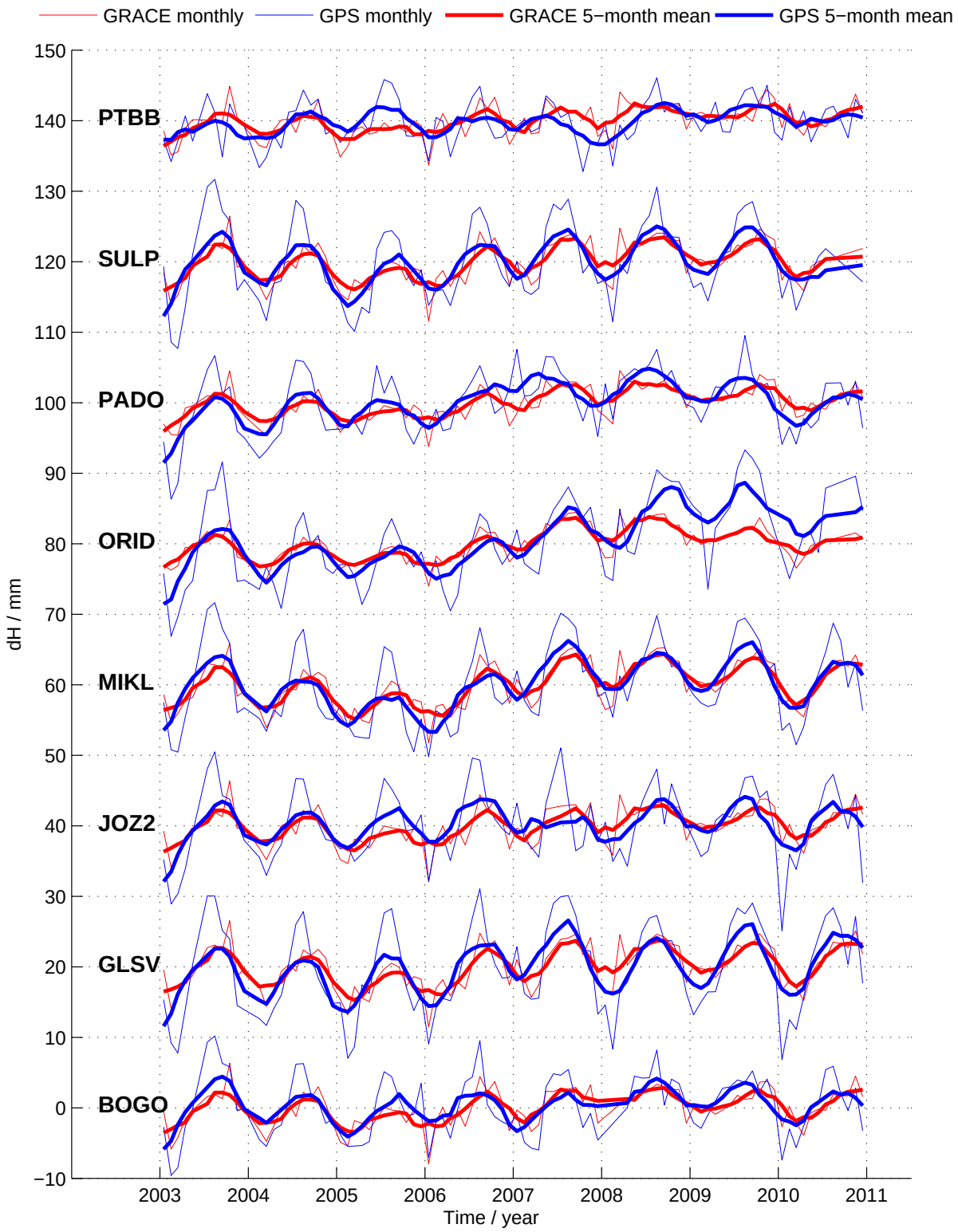

Figure 4.5: *Comparisons of height deformation time series from GRACE and GPS in Danube area*

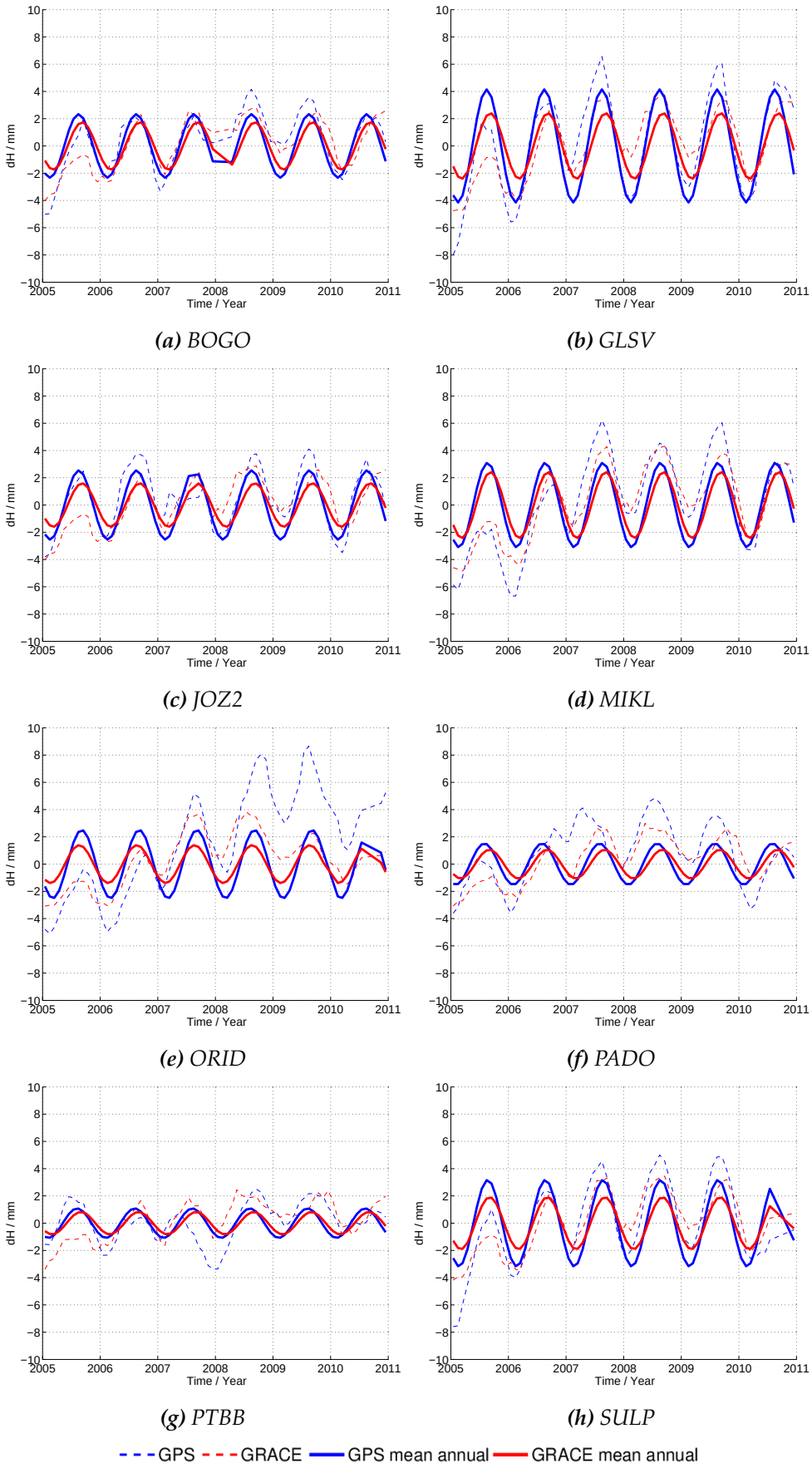

Figure 4.6: *Annual mean height deformation time series from GRACE and GPS in Danube area*

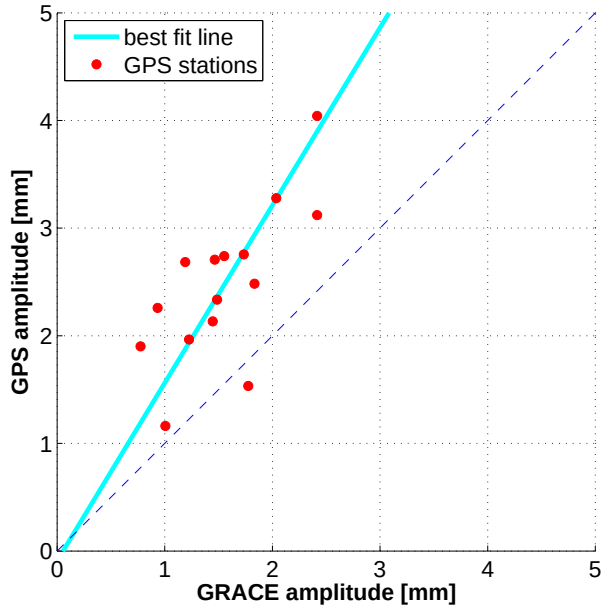

Figure 4.7: *Comparisons of vertical annual amplitudes of signals from GRACE and GPS*

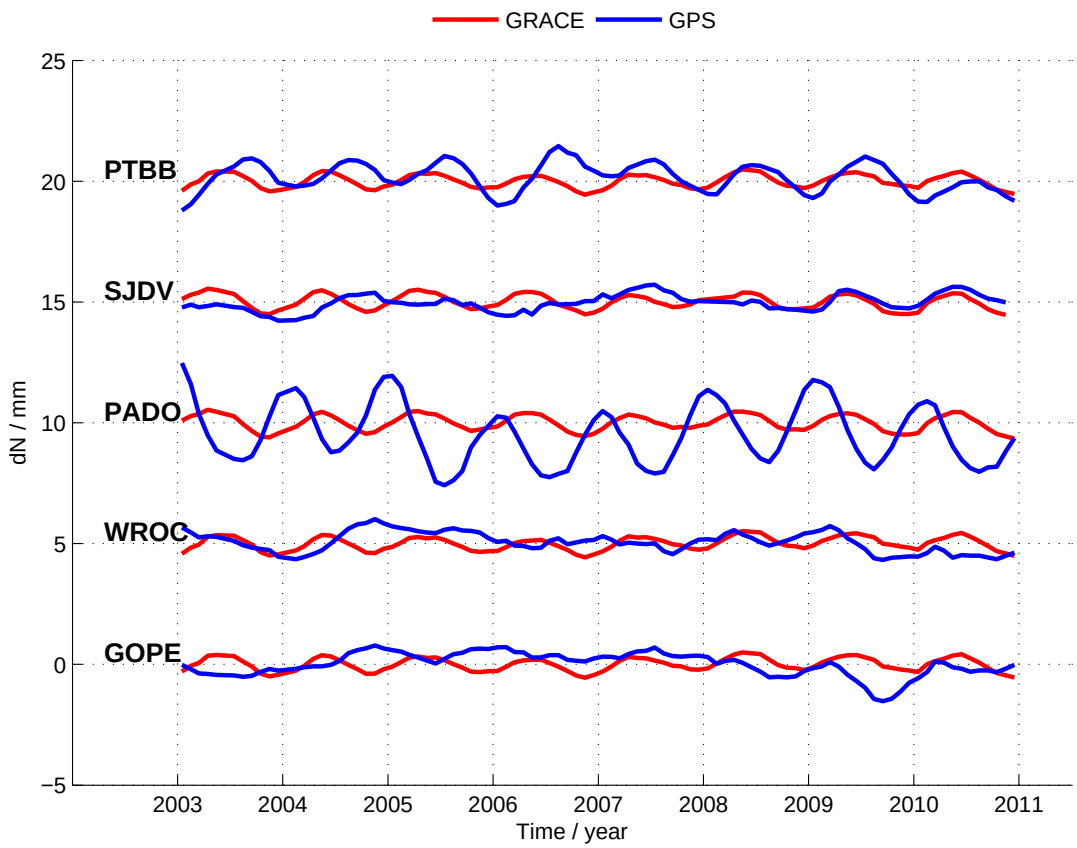

Figure 4.8: *Northward deformation time series of from GRACE and GPS in Danube area*

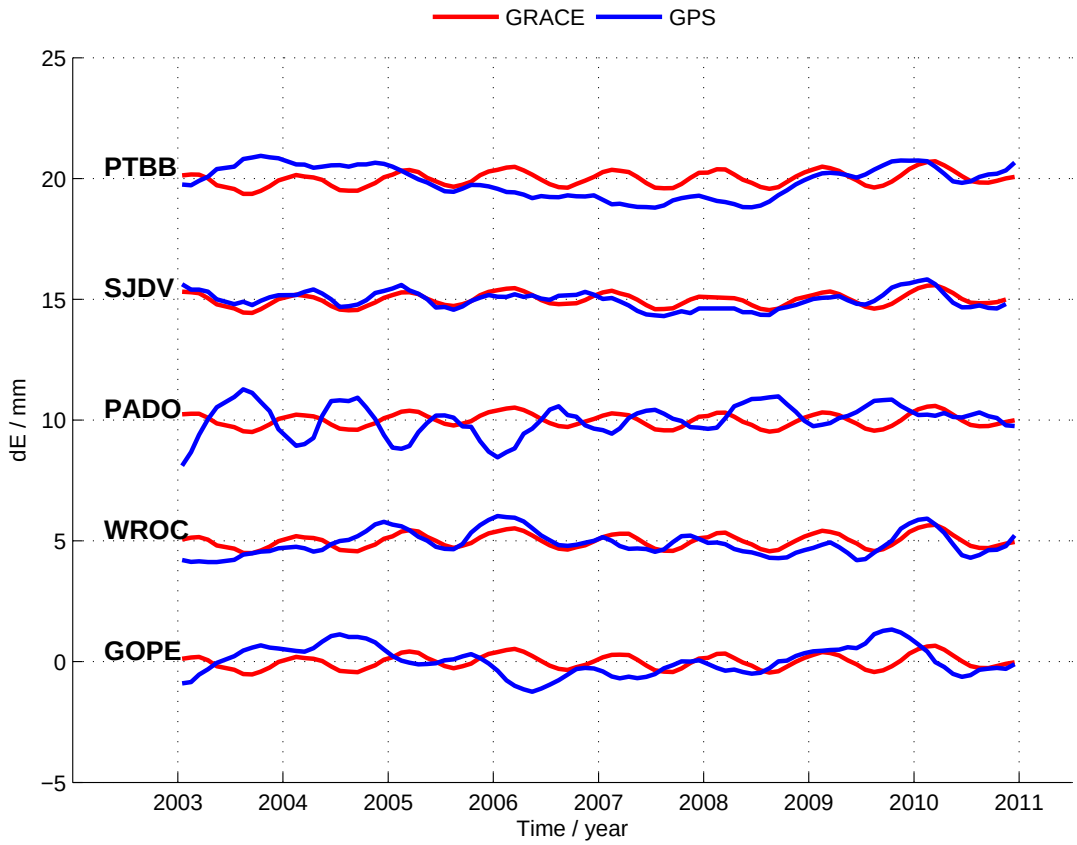

Figure 4.9: *Eastward deformation time series of from GRACE and GPS in Danube area*

Table 4.5: *Northward deformation comparisons in terms of statistical coefficients*

Station	Correlation Coefficient	WRMS Reduction (%)	Nash-Sutcliffe Coefficient
BOGO	-0.35	-24.3	-0.23
BOR1	-0.20	-16.8	-0.46
GLSV	0.35	6.5	-0.30
GOPE	-0.10	-19.2	-0.08
JOZ2	-0.20	-22.8	-0.19
JOZE	0.26	0.38	-0.55
MIKL	-0.01	-15.1	0.12
ORID	0.09	-1.5	-0.01
PADO	-0.09	-5.1	0.09
POTS	-0.13	-26.1	-0.81
PTBB	0.33	4.6	-1.12
SJDV	0.15	-23.9	-0.91
SULP	0.18	-4.2	-0.44
WROC	-0.01	-18.7	-0.36
ZIMM	-0.01	-34.9	-0.24

From the WRMS reductions shown in tables, it can also state that deformation time series from both two geodetic observation techniques do not have the consistent performance. Most of these stations have negative WRMS reduction, that means the WRMS of GPS after removing GRACE become larger.

From NSE coefficients with negative values, it also reflects that there are great discrepancies of deformation amplitudes of most stations in horizontal direction.

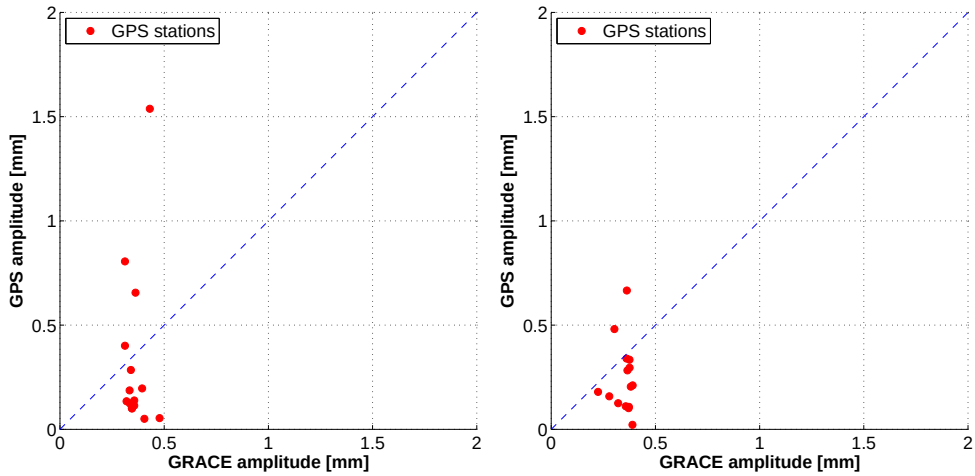

(a) *Northward* ***(b)*** *Eastward*

Figure 4.10: *Comparisons of horizontal annual amplitudes of signals from GRACE and GPS*

Nevertheless, different from other stations in east, the deformations of SJDV and WROC stations derived from GRACE are highly correlated with deformations observed by GPS with correlation above 0.5, and have acceptable WRMS reduction after removing GRACE from GPS

Table 4.6: *Eastward deformation comparisons in terms of statistical coefficients*

Station	Correlation Coefficient	WRMS Reduction (%)	Nash-Sutcliffe Coefficient
BOGO	0.13	-6.3	-0.14
BOR1	-0.15	-32.5	-0.76
GLSV	0.07	-4.0	-0.08
GOPE	-0.25	-21.5	-0.48
JOZ2	-0.14	-26.5	-0.61
JOZE	0.29	2.55	0.04
MIKL	-0.08	-16.7	-0.37
ORID	-0.17	-4.8	-0.10
PADO	-0.71	-33.7	-0.79
POTS	-0.07	-41.3	-0.99
PTBB	-0.05	-12.9	-0.34
SJDV	0.64	21.9	0.39
SULP	-0.07	-23.3	-0.60
WROC	0.54	15.1	0.25
ZIMM	0.01	-17.7	-0.41

comparing with other stations, which reveals in east direction deformations of these two stations from GRACE and GPS have not good but acceptable consistency.

In figure 4.8 and 4.9, monthly deformations in north and east of five stations are shown. Some stations shown in this figure have obvious annual behaviors while some do not have, especially the time series from GPS. Although some stations have annual signals from both GRACE and GPS, the time series represent totally opposite to each other with negative correlations.

That is to say, the horizontal deformations in Danube area mostly show extremely low correlations and very bad consistency between GPS and GRACE, depending on the distinct inconsistent monthly annual time series in north and east.

The mean annual amplitudes from all 15 stations in figure 4.10 are plotted to compare the annual amplitudes in horizontal direction from GRACE and GPS. Only if all the GPS annual signals have completely same amplitudes, then those dots are on the best fit line. From figure 4.10, it notes that most of stations have lager amplitudes of deformations from GPS than from GRACE, while a few of stations have distinctly much larger amplitudes from GPS than from GRACE. However, compared with the vertical components, the amplitudes from GPS and GRACE are both quite tiny, which indicates that loading deformations happened primarily in vertical and the signal of GPS contains some local effects in horizontal direction.

4.3.3 Disagreement Analysis between GRACE and GPS

As shown in figure 4.11(a), the MIKL station (http://sopac.ucsd.edu/sites/), which locates in Mykolaiv, Ukraine , has nearly perfect consistency between vertical deformations from GRACE and GPS. The comparison shows high correlation, large WRMS reduction after

removing GRACE from GPS signal, and small discrepancy of annual amplitudes which can be seen in the figure 4.11(b). This great consistency may result from the geographical location of this IGS station. From figure 4.11(c), the station can be seen located at the estuary of Black Sea with large continental water storage nearby.

Hence, the dominant influence for this station may come from the loading variation of Black Sea, so that it induces quite strong seasonal deformations over eight years. For GRACE, the water loading variation would results in gravity variation in this area and appears in form of surface deformations; for GPS, the surface displacements driven by water loading variation can be observed as geometric coordinate changes.

As shown in figure 4.12(a), the ORID station (http://sopac.ucsd.edu/sites/), which locates in Ohrid, Macedonia, has not so good consistency between vertical deformations from GRACE and GPS, especially from 2008. The comparison shows high correlation, medium WRMS reduction after removing GRACE from GPS signal, and large discrepancy of annual amplitudes shown in the figure 4.12(b). The geographical location of this IGS station also plays an important role in deformation analysis. From figure 4.12(c), the station can be seen located near two interior lakes.

Therefore, the roughly annual patterns of vertical deformations of this station may mainly due to the water loading variation of two lakes. From 2003 to 2008, it has strongly seasonal deformations at this station and the disagreement between GRACE and GPS is tiny. So we can assume that, during this period, the surface deformations are driven by the hydrological loading variation from nearby two lakes. However, since 2008 the disagreement becomes larger. The reason may refer to the unknown errors in GPS signal or the neglected interannual deformations that GRACE cannot measured. In figure 4.12(b), the discrepancy of annual mean amplitudes can also prove the possibility assumed above.

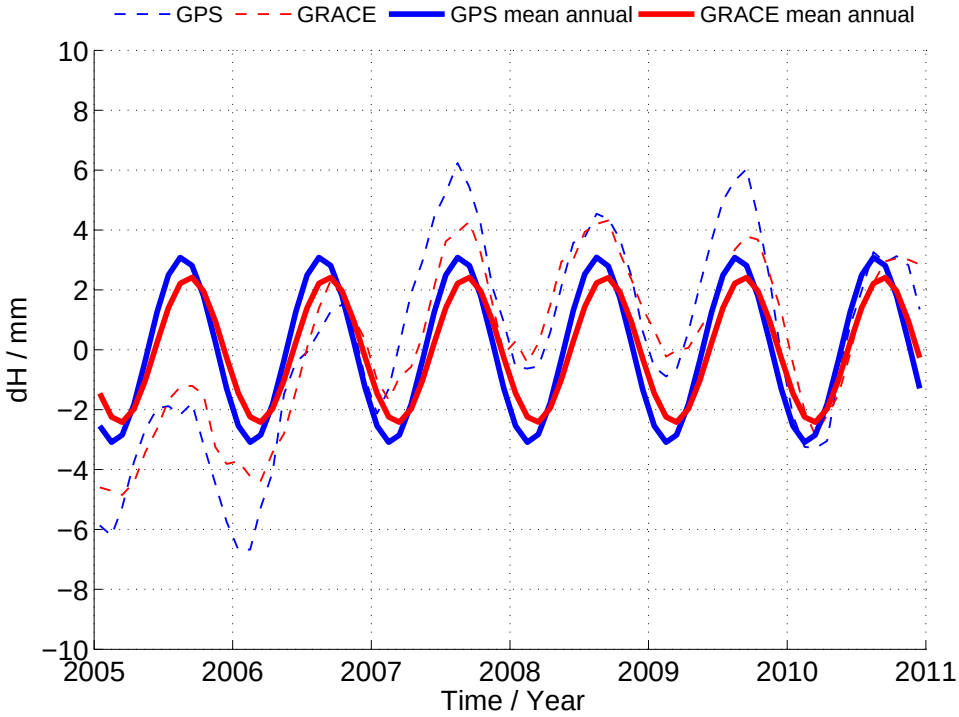

(a) *Annual mean height deformations*

(b) *Site location*

Figure 4.11: *Monthly and annual mean height deformation of site Mykolaiv (MIKL) in Ukraine*

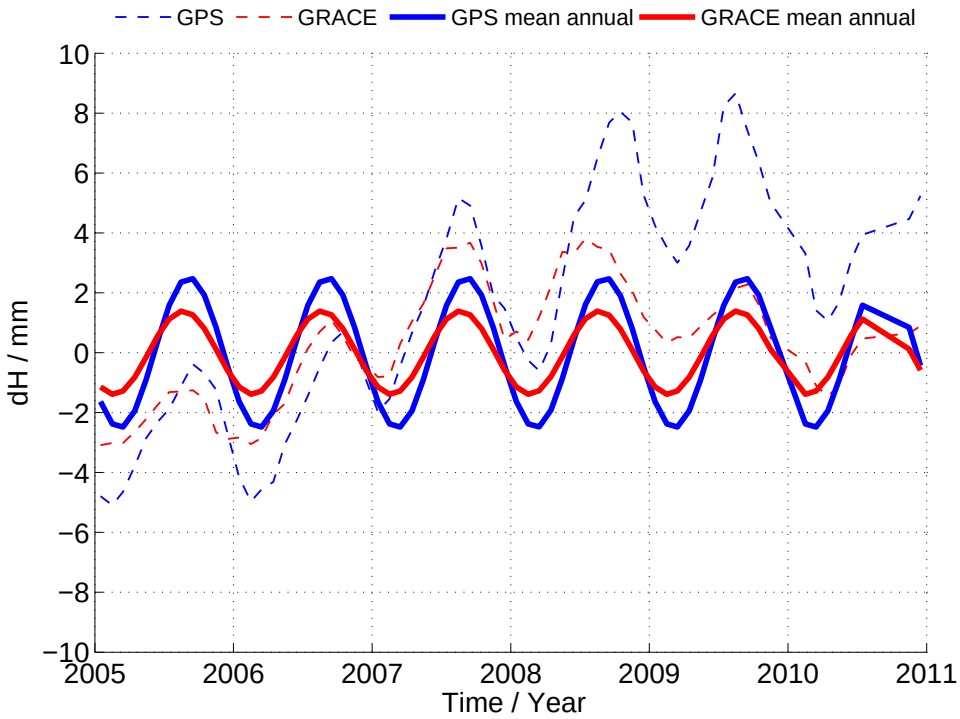

(a) *Annual mean height deformations*

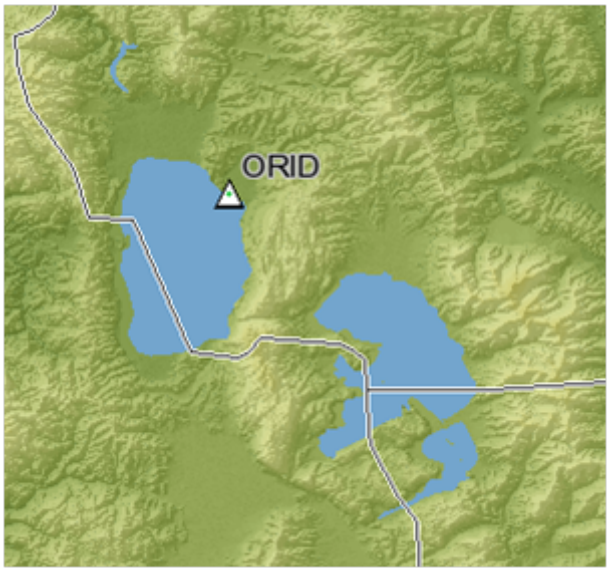

(b) *Site location*

Figure 4.12: *Monthly and annual mean height deformation of site Ohrid (ORID) in Macedonia*

In figure 4.13(a), at the PTBB station (http://sopac.ucsd.edu/sites/) which locates in Braunschweig, Germany, there are obviously annual vertical deformations from 2003 to 2008 though the annual patterns are not consistent between GRACE and GPS. These two kinds of observations show high correlation and little discrepancy of mean annual amplitudes shown in figure 4.13(b), however, there is still large disagreement between GRACE and GPS that the WRMS reduction after removing GRACE from GPS signal is quite little. Comparing the annual mean with monthly deformations, the annual mean signals cannot exactly report the inconsistency since the annual deformations are not the same every year as a result of environmental influences.

To find the implicit reason, the location of this IGS station should be considered. From figure 4.13(c), the station locates inland where there is no continental water storages around station. Due to this fact, the influences on this station come not only from the hydrological loading variation but also other factors. The annual mean amplitude is only 1 mm, which is smaller than the amplitudes of other stations. It can also mediately reflect that there is no continental water storage nearby so that the surface load variation ranges quite small.

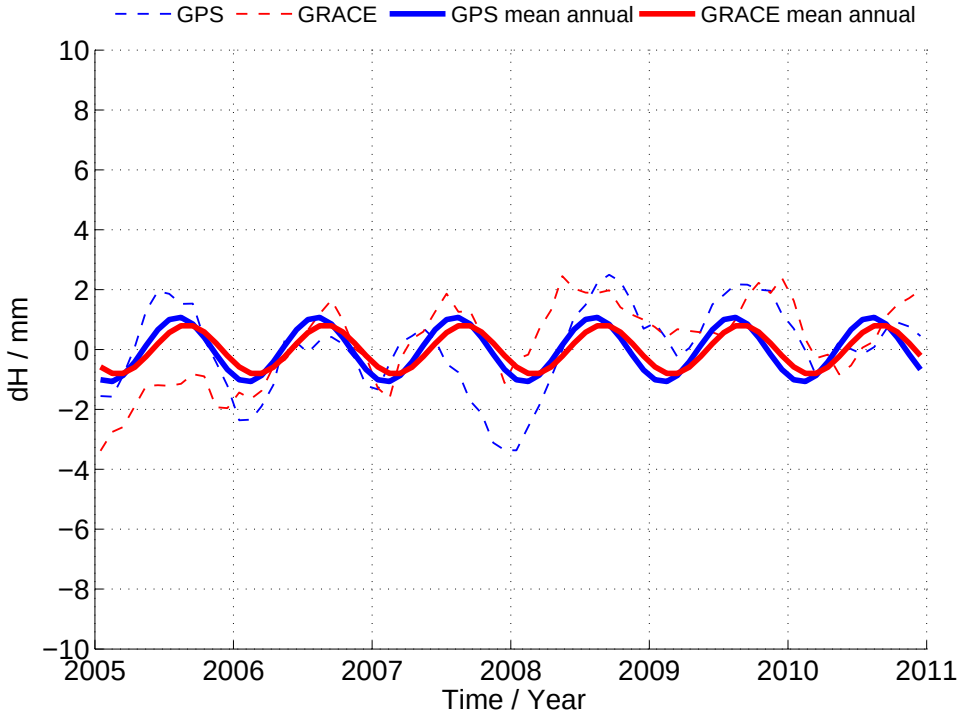

(a) *Annual mean height deformations*

(b) *Site location*

Figure 4.13: *Monthly and annual mean height deformation of site Braunschweig (PTBB) in Germany*

The SJDV station (http://sopac.ucsd.edu/sites/), which locates in Saint Jean des Vignes, France, has really bad consistency between vertical deformations from GRACE and GPS as shown in figure 4.14(a). The comparison shows very low correlation, WRMS increase after removing GRACE from GPS signal, and large discrepancy of annual amplitudes which can be seen in the figure 4.14(b). From the figure 4.14(a), even the annual patterns cannot be clearly seen for both GPS and GRACE.

Thus, the geographical location of this IGS station have to be taken into account when we analyze the inconsistency between GPS and GRACE. From figure 4.14(c), the station located in hilly land where full of mountains circle around.

As a result of its location, the continental water loading variation is not possibly to be the dominant influence of the surface displacements at this station. That is to say, the deformations observed by GPS are driven not mainly by the hydrological loading variation, so that they are consequently not relevant to the deformations derived from GRACE. Therefore, the implicit reason of inconsistency might be supposed that the seasonal loading variation is not the primary driven effect.

The monthly vertical deformations of the arbitrary five stations are visualized together in figure 4.11 in order to testify the relevancy of these stations in Danube area.

In figure 4.5, the five stations act obviously common annually repeating patterns, that the deformations rise up between spring and autumn, and fall down between autumn and spring. From the periodical patterns of deformations, it strongly supports the assumption that the annual deformations might be driven by climate changes.

Therefore, it might be supposed that the surface loading becomes larger from autumn induced deformations falling down when the weather gets warm, and then gradually declines from spring caused deformations rising up when it gets cold. That reveals these chosen five stations are strongly influenced by seasonal loading variation, which could be regarded mainly due to hydrological effects.

In figure 4.8 and 4.9, for most of stations the horizontal deformations have large disagreement between GRACE and GPS, even though some stations preform quite consistent annual patterns, like SJDV and WROC in east direction. Comparing with vertical deformations in 4.5, the magnitude of horizontal deformations are one order lower than vertical deformations. Furthermore, the deformations in north and east of five arbitrary stations do not show clearly common seasonal patterns, especially the deformations from GPS.

From the performance in the figure, we might assume that both GPS and GRACE cannnot reflect exactly the annual loading deformations in horizontal direction, due to the fact that GRACE is not sensitive to the lateral displacements while GPS horizontal observations are influenced by many complicated effects. In other word, it may be supposed that vertical deformations strongly sense the seasonal surface loading variation in Danube area.

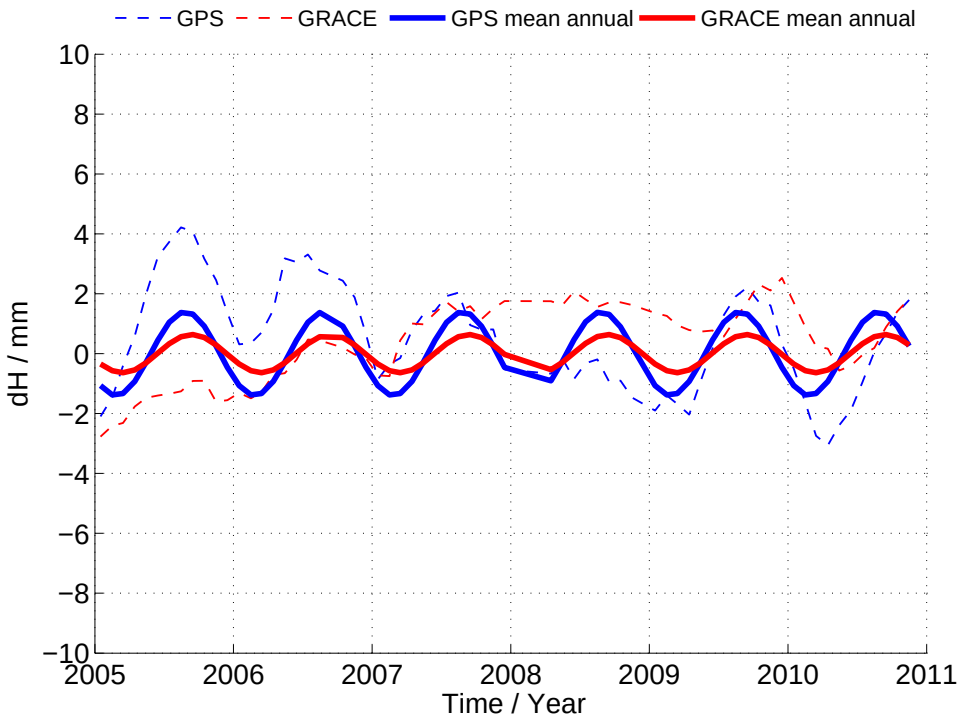

(a) *Annual mean height deformations*

(b) *Site location*

Figure 4.14: *Monthly and annual mean height deformation of site Saint Jean des Vignes (SJDV) in France*

4.4 The Great Lakes Area

In the Great Lakes Area, 8 IGS stations located around the five lakes will be analyzed. And the locations of these stations are shown as below:

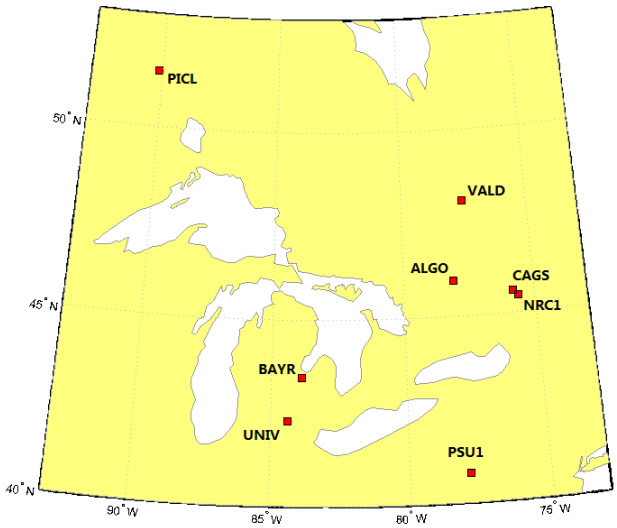

Figure 4.15: *IGS Stations in the Great Lakes Area*

4.4.1 Vertical Deformation Time Series Comparisons

Like in chapter 4.2.1, the vertical deformations are derived by equation (3.26), and the spatial and temporal reference frame are unified as described in chapter 3.2.4. By means of correlation coefficient, WRMS reduction and NSE coefficient, the disagreements between two geodetic observation techniques can be successfully evaluated. The detailed statistical results are listed in table 4.7.

Table 4.7: *Vertical deformation comparisons in terms of statistical coefficients*

Station	Correlation Coefficient	WRMS Reduction (%)	Nash-Sutcliffe Coefficient
ALGO	0.79	30.1	0.51
BAYR	0.62	20.9	0.36
CAGS	0.64	15.8	0.28
NRC1	0.77	24.0	0.42
PICL	0.67	21.4	0.37
PSU1	0.64	20.3	0.35
UNIV	0.68	24.0	0.42
VALD	0.65	20.2	0.35

From table 4.7, the 8 stations in Great Lakes area show quite high correlations in vertical direction, which are all above 0.5, while the WRMS reductions after removing GRACE from GPS range from 15% to 30%. Only one station has less than 20 percent WRMS reduction, which indicates the deformations derived from GRACE are not as consistent to the deformations observed by GPS as we expect. From NSE coefficients, all the stations have positive values, which can reveal that the vertical deformations of these stations have small disagreements between GRACE and GPS.

Later in chapter 4.4.3, the analysis of vertical deformations of some representative stations will be discussed in detail.

The monthly deformations of eight stations shown in the figure 4.16 have clearly annual patterns from 2003 to 2008, as well as the mean annual deformation time series are shown in figure 4.18. In order to avoid noisy signal and allow a meaningful plot, the time series have been both smoothed in five-month scale. The mean annual deformations are calculated by average of eight years. With mean annual deformations from and GPS, a discrepancy between GPS and GRACE is still existed.

To compare the annual amplitudes of GPS with GRACE in vertical direction, the mean annual amplitudes from 8 stations are distributed in figure 4.17. As is shown in the figure, all the points locate in the upper triangular area. Hence, it can be interpreted that deformations from GPS have commonly larger annual amplitudes than from GRACE. Besides that, from the figure 4.17, a slight phase shift about 30 days can be obviously seen between GRACE and GPS.

4.4.2 Horizontal Deformation Time Series Comparisons

In figure 4.19 and 4.20, deformations in north and east of four arbitrary stations are shown. Those stations show roughly annual patterns but polytropic amplitudes. The northward deformations from GPS and GRACE have more or less consistency over eight years. However, in east direction no obvious relevancy existed between GPS and GRACE.

The horizontal deformations have been compared in terms of correlation coefficient, WRMS reduction and NSE coefficient. The results are listed in table 4.8 and table 4.9.

From table 4.8 and 4.9, comparing with vertical deformations, in north direction most of stations show positive but low correlations while in east nearly all the stations show negative correlations, which indicates that in horizontal direction deformations from GRACE and GPS are not well correlated.

From the WRMS reductions shown in two tables, we can see in north the WRMS of deformations from GPS do not reduce largely after removing GRACE from GPS, while in east the WRMS even increase after removing GRACE signal, that reveals the horizontal deformations from GRACE and GPS have large disagreement.

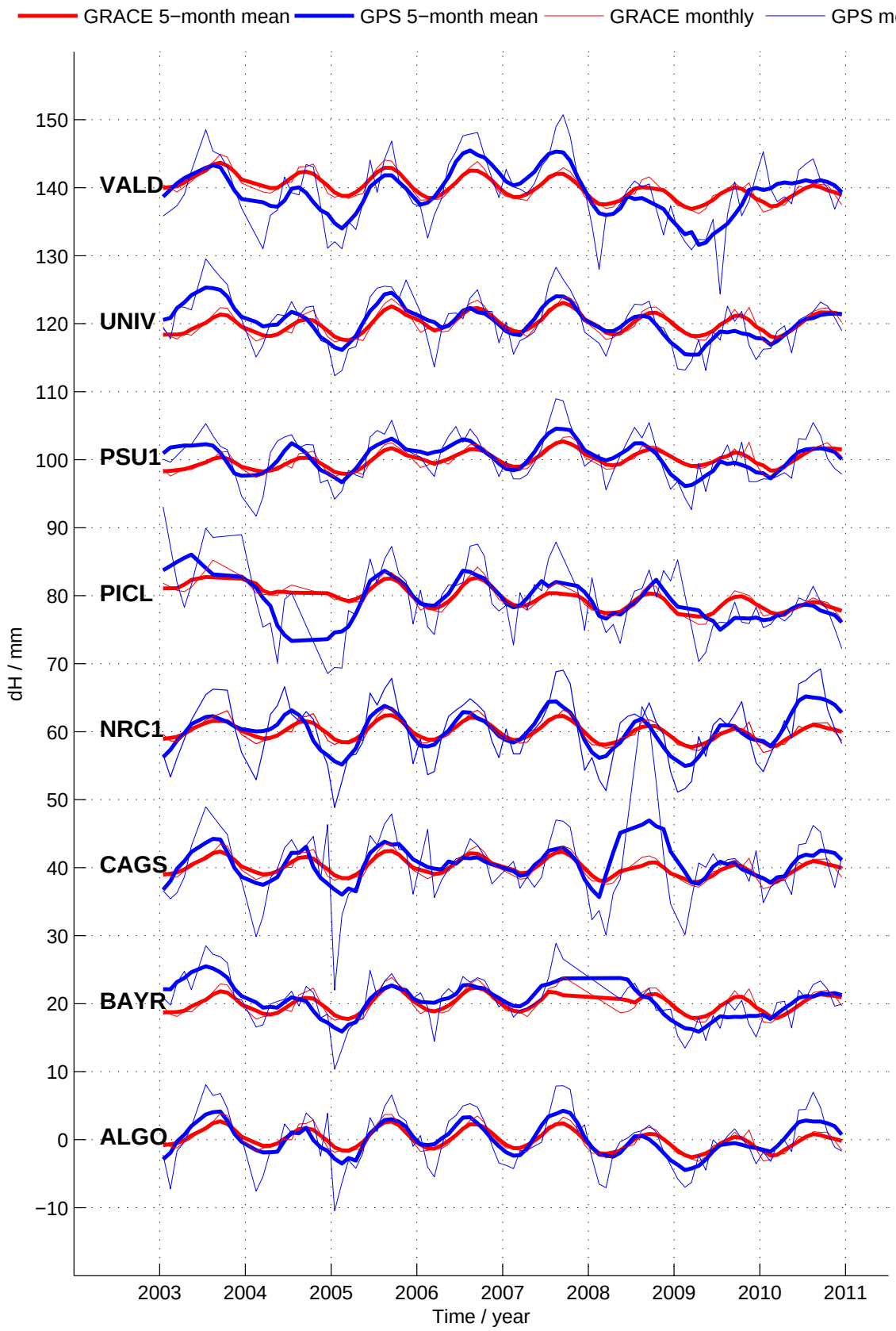

Figure 4.16: *Comparisons of height deformation time series from GRACE and GPS in Great Lake Area*

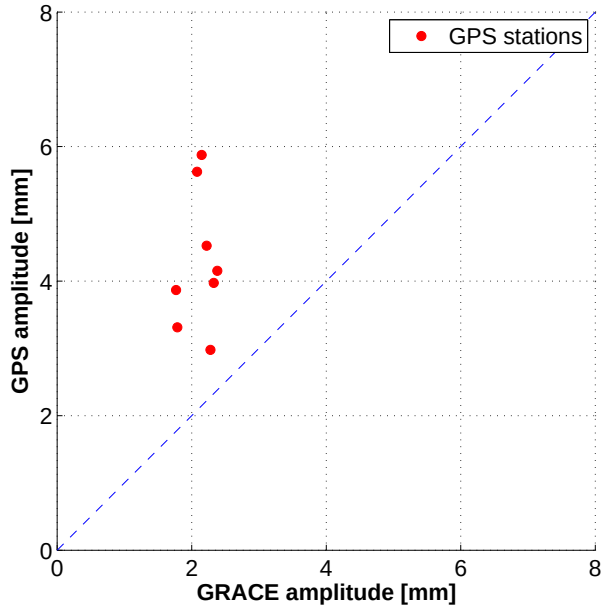

Figure 4.17: *Comparisons of annual amplitudes of signals from GRACE and GPS*

Besides that, from NSE coefficients with values around 0, it reflects that for most stations there are large discrepancies of deformation amplitudes between GRACE and GPS in both north and east.

Table 4.8: *Northward deformation comparisons in terms of statistical coefficients*

Station	Correlation Coefficient	WRMS Reduction (%)	Nash-Sutcliffe Coefficient
ALGO	0.42	8.5	0.07
BAYR	0.62	18.9	0.19
CAGS	0.12	0.6	0.02
NRC1	-0.05	-4.3	-0.01
PICL	0.32	3.1	0.01
PSU1	0.23	2.6	-0.04
UNIV	0.65	20.8	0.17
VALD	0.46	6.13	0.03

In brief, the horizontal deformations especially in east mostly show extremely low correlations and very bad consistency between GPS and GRACE in Great Lakes area.

What is more, the mean annual amplitudes from all 8 stations in figure 4.21 are plotted to compare the annual amplitudes in horizontal direction from GRACE and GPS. From figure 4.21, it shows that the annual amplitudes of deformations from GPS are averagely larger than from GRACE. That illustrates that the signal observed by GPS contains local effects as well. However, compared with the vertical components, the amplitudes from GPS and GRACE are quite small, which are not larger than 2 mm. As a result, it indicates that surface loading has tiny impact on horizontal components but large impact on vertical components.

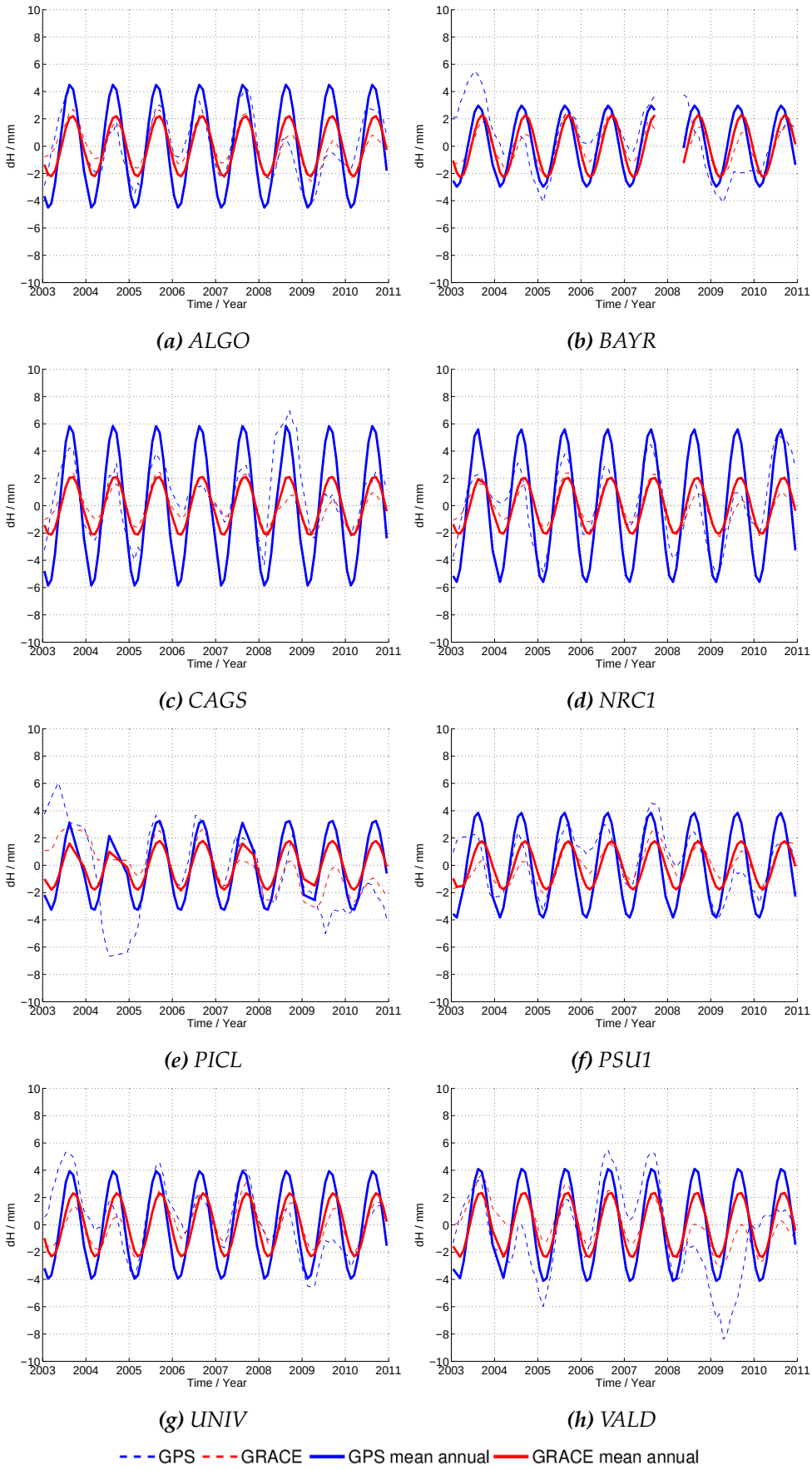

Figure 4.18: *Annual mean height deformation time series from GRACE and GPS in Great Lakes area*

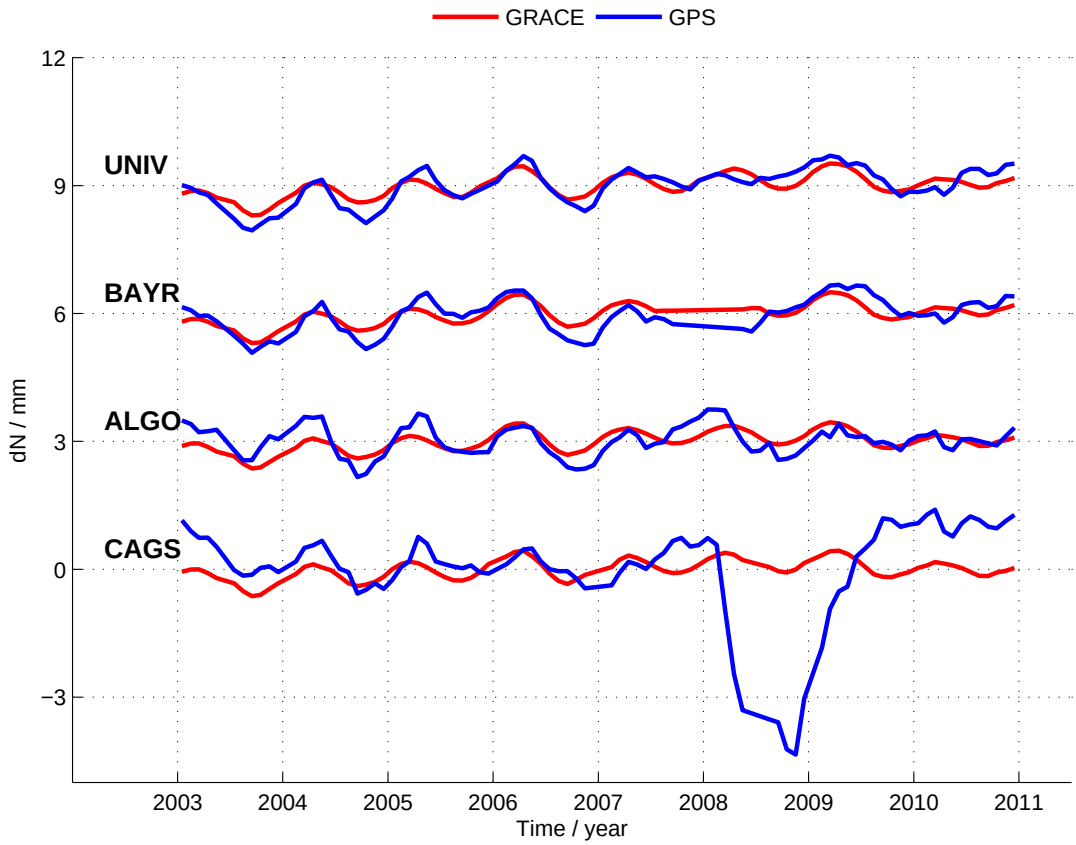

Figure 4.19: *Northward deformation time series of from GRACE and GPS in Great Lakes area*

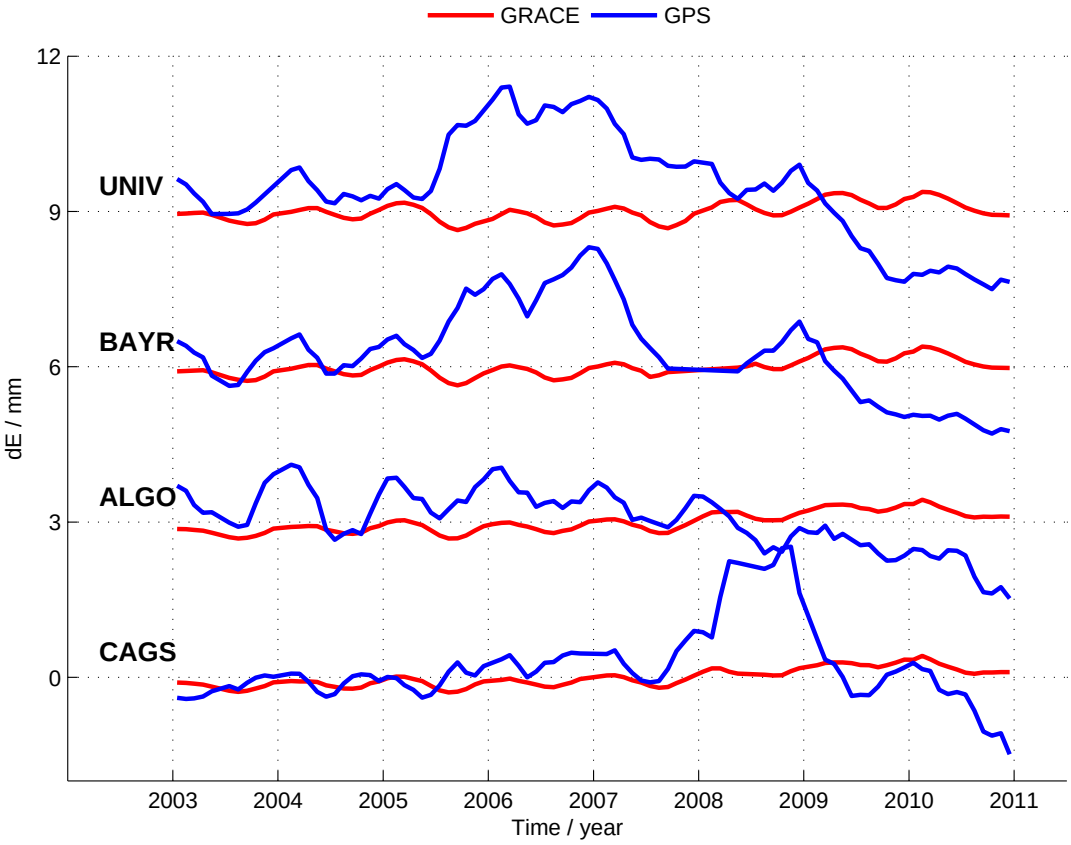

Figure 4.20: *Eastward deformation time series of from GRACE and GPS in Great Lakes area*

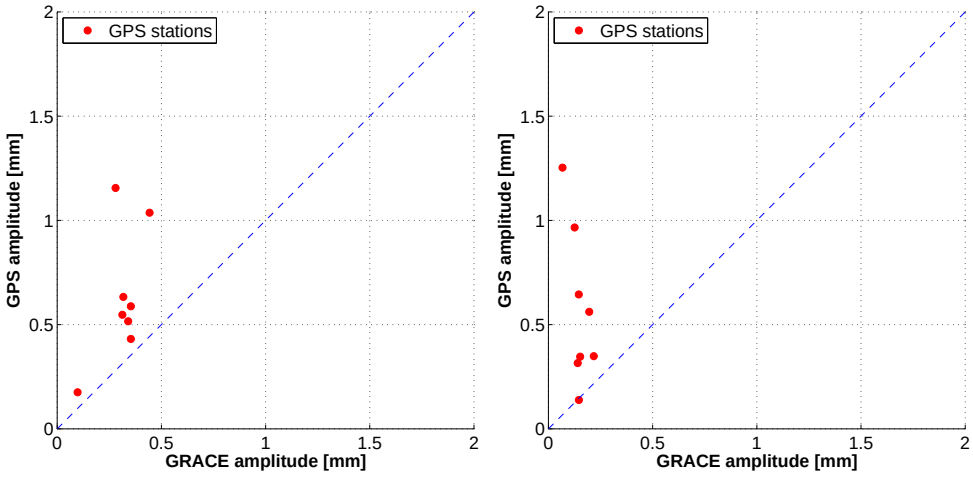

(a) *Northward* ***(b)*** *Eastward*

Figure 4.21: *Comparisons of horizontal annual amplitudes of signals from GRACE and GPS*

Table 4.9: Eastward deformation comparisons in terms of statistical coefficients

Station	Correlation Coefficient	WRMS Reduction (%)	Nash-Sutcliffe Coefficient
ALGO	-0.11	-4.6	-0.10
BAYR	-0.21	-5.2	-0.19
CAGS	0.06	-0.3	-0.02
NRC1	-0.14	-2.9	-0.08
PICL	-0.07	-2.9	-0.06
PSU1	-0.16	-3.3	-0.10
UNIV	-0.27	-5.35	-0.24
VALD	0.02	-0.84	-0.03

4.4.3 Disagreement Analysis between GRACE and GPS

The vertical deformations of all eight stations are visualized together in figure 4.16 in order to testify the relevancy of these stations in Great Lakes area.

In figure 4.16, the eight stations have clearly common annual repeating patterns, that the peak value of deformations is always in summer and valley value in winter, even though the GPS deformations at some stations have anomalous behaviors. Since the height deformations show seasonal patterns, these eight stations are supposed to be strongly influenced by seasonal loading variation from hydrological changes.

In figure 4.19 and 4.20, here the northward and eastward deformations of four stations are shown. In north, although all the four stations show common annual repeating patterns, there is still large disagreement between GRACE and GPS, especially the CAGS station, of which in 2008 the deformations observed by GPS have an anomalous declination (figure 4.19). In east, large disagreement between GPS and GRACE can be seen (figure 4.20). Also, there is no clearly annual patterns for deformations from GPS. The deformations derived from GRACE are spatially smoothed with about 350 km spatial resolution, while the deformations observed by GPS are discrete points on the globe. In this area, all the eight stations are very close to each other. Hence, the disagreement between GPS and GRACE might due to the inconsistent spatial resolution. GRACE is not sensitive to the lateral displacements, but GPS horizontal observations are influenced by many complicated effects. From the figure 4.19 and 4.20, we cannot expect better in horizontal direction, comparing to vertical deformations. In other words, it may be concluded that vertical deformations are supposed to significantly reflect the seasonal surface loading variation in Great Lakes area.

To particularly illustrate how the spatial resolution influences the loading induced deformations in Great Lakes area, two examples will be listed in figure 4.22 and 4.23.

As is shown in figure 4.22c, two IGS stations, BAYR and UNIV, locate at Saginaw and Jackson respectively in Michigan, USA (http://sopac.ucsd.edu/sites/). The BAYR station is along the side of the Huron lake, and UNIV station is about 130 km south to BAYR. In figure 4.22a, both

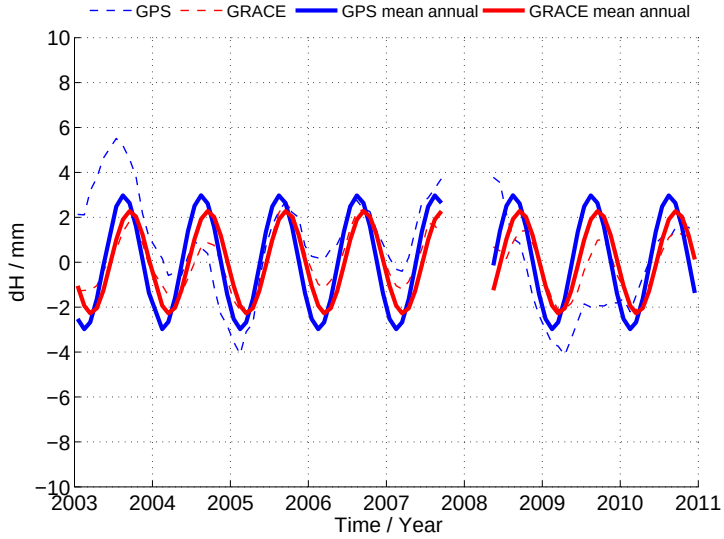

(a) *Annual mean height deformations (BAYR)*

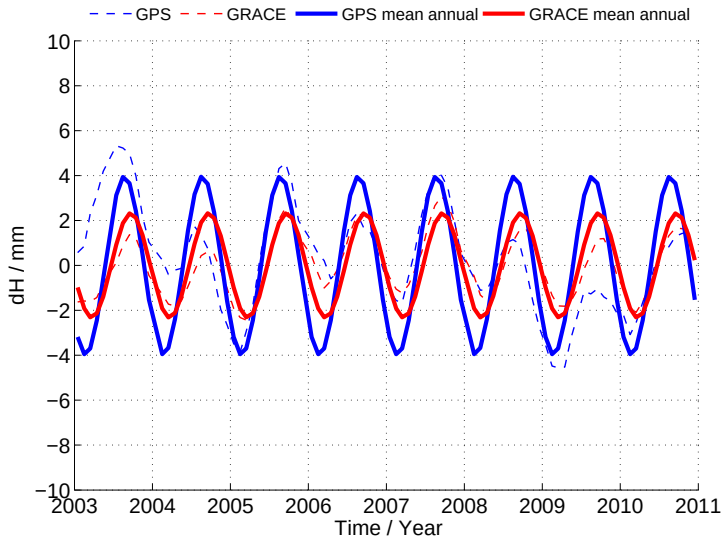

(b) *Annual mean height deformations (UNIV)*

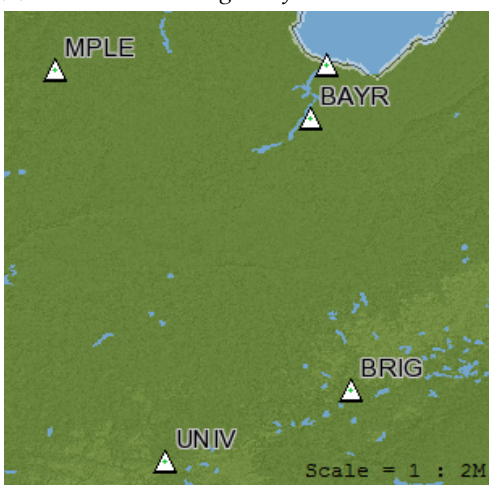

(c) *Station location*

Figure 4.22: *Monthly and annual mean height deformations of site Saginaw (BAYR) (upper) and Jackson (UNIV) (lower) in Michigan, USA*

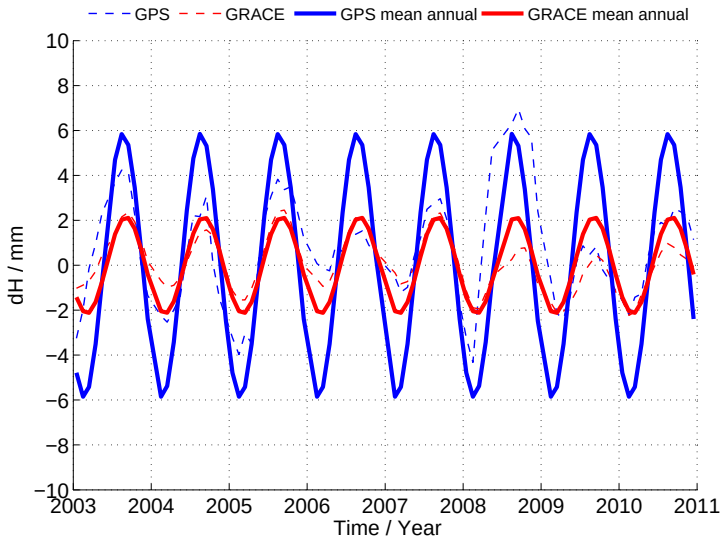

(a) *Annual mean height deformations (CAGS)*

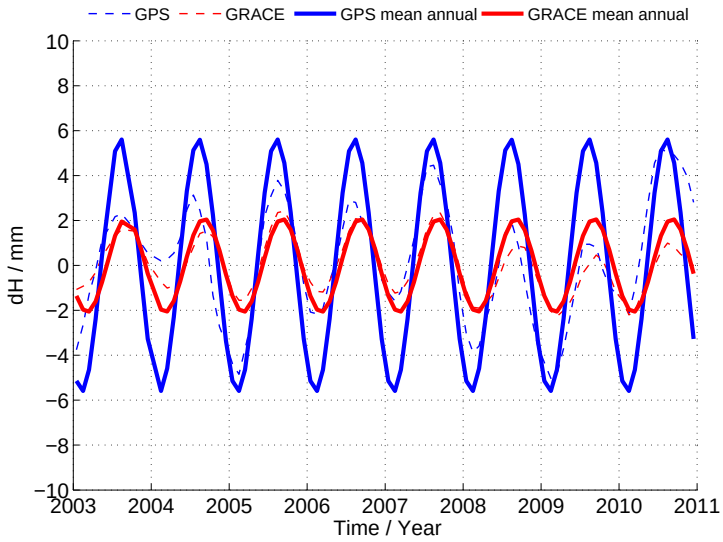

(b) *Annual mean height deformations (NRC1)*

(c) *Station location*

Figure 4.23: *Monthly and annual mean height deformations of site Gatineau (CAGS) (upper) and Ottawa (NRC1) (lower) in Canada*

of two stations show high correlations but not a good consistency in vertical deformations between GRACE and GPS. The implicit reason of the inconsistency might refer to the unknown errors in GPS signals such as the atmospheric effects, or the neglected tectonic motions that GRACE cannot detect. The deformations from GPS of each two stations have synchronous annual repeating patterns and so do deformations from GRACE, that indicates strong coherency of these two stations. However, the mean annual amplitudes of two stations are slightly different, which is visualized in figure 4.22b. This phenomenon can be interpreted that BAYR is much closer to the Huron lake, and the seasonal hydrological loading variation dominate the surface deformation much more than any other influences. Therefore, from the mean annual amplitudes, there is much less discrepancy between GPS and GRACE for BAYR than UNIV due to the different geographical locations.

In figure 4.23c, two IGS stations, CAGS and NRC1, locate at Gatineau and Ottawa respectively in Canada (http://sopac.ucsd.edu/sites/). The CAGS and NRC1 stations are in northeast of the Ontario lake, about only 40 km apart from each other. In figure 4.23a, although two stations with quite high correlations in vertical deformations, the large disagreement still exists between GRACE and GPS. The anomalous phenomenon is that, the deformations from GRACE of two stations seem to have the same annual patterns, but the deformations of these two stations from GPS are not consistent. The only explaination of such phenomenon is due to the limited spatial resolution of GRACE. Since these two stations are apart less than 100 km from each other, the vertical surface deformations derived from GRACE then show the same performances. However, in fact, at these two stations the surface deformations have not exactly the same annual patterns, and the slight difference in 2008 could be observed by GPS but is not capable to captured by GRACE. On the other side, the undetected deformations in 2008 are not visible in mean annual signal, so the mean annual amplitudes shown in figure 4.23b are nearly the same for two stations. Whatever, the similar common annual repeating patterns certify the coherency of loading induced surface deformations at these two stations.

In short, the different spatial resolution play an important role on small-scale regional surface deformations analysis, and still needs to be taken into consideration in the evaluation of consistency between GRACE and GPS.

4.5 Filter Sensitivity Test

Due to the fact that filtering always plays an important role in GRACE data pre-processing, it is essential to evaluate how much the influences of different filters on the deformations derived from GRACE. Therefore, the performances of different type of filters would be discussed in this chapter, and nine different filter schemes are involved (in table 4.10).

Table 4.10: Parameters of filter schemes

Filter Type	Radius	
Isotropic Gaussian filter	500 km	300 km
Anisotropic Gaussian filter	500 km	300 km
Destriping + isotropic Gaussian filter	500 km	300 km
Destriping + anisotropic Gaussian filter	500 km	300 km
Stochastic filter		

We choose the European area as an example, and process the period of loading deformations from 2005 to 2010. The mean annual deformations within 6 years can be obtained from the deformation time series from GRACE, and then the mean annual amplitudes filtered by different filter combinations are visualized in figure 4.24 – 4.27.

Compared with the figure 4.24 – 4.27, the signals between Gaussian and Wiener filter show a distinct difference in Europe, especially in the Danube river basin. The mean annual deformations in Danube area have larger amplitudes in figure 4.28. The reason might be that the signal filtered by Wiener filter maintains more loading information, which is averaged by Gaussian smoothing.

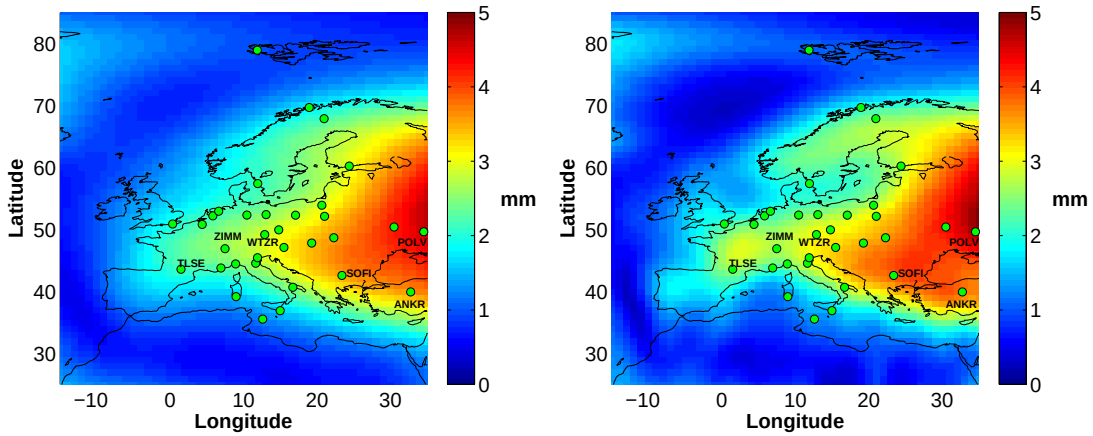

***(a)** 500 km* ***(b)** 300 km*

***Figure 4.24:** mean annual amplitudes of vertical deformations in Europe filtered by Gaussian isotropic filter*

To show the differences among different filter schemes graphically, the deformation time series from GRACE of 40 selected stations are compared with GPS, and the disagreements between GRACE and GPS are evaluated in terms of correlation coefficients and weight root mean square (WRMS) reductions. Before comparisons, the spatial and time reference frame have been unified as previous work.

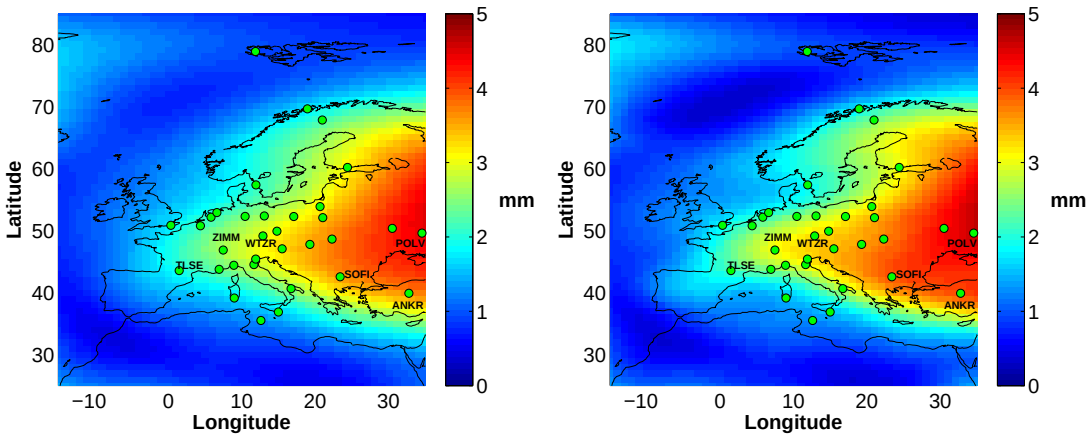

(a) 500 km *(b) 300 km*

Figure 4.25: *mean annual amplitudes of vertical deformations in Europe filtered by combination of Gaussian isotropic and destriping filter*

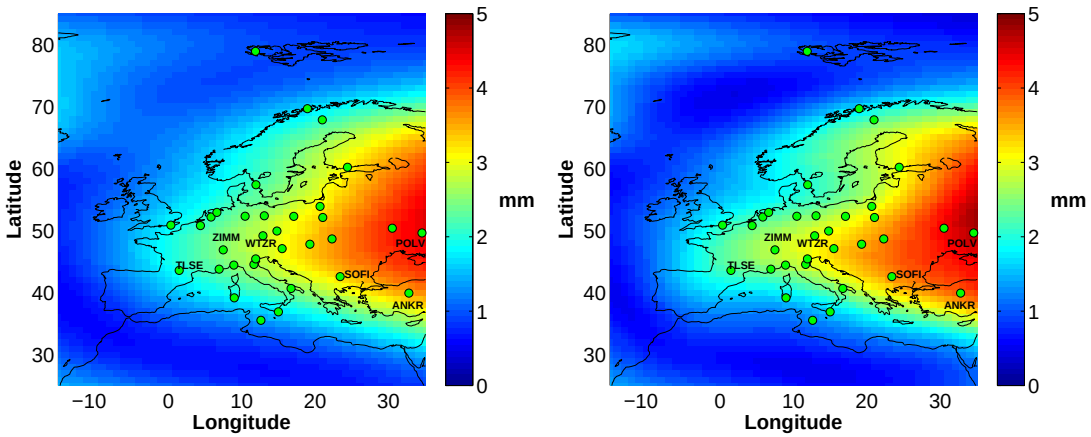

(a) 500 km *(b) 300 km*

Figure 4.26: *mean annual amplitudes of vertical deformations in Europe filtered by Gaussian anisotropic filter*

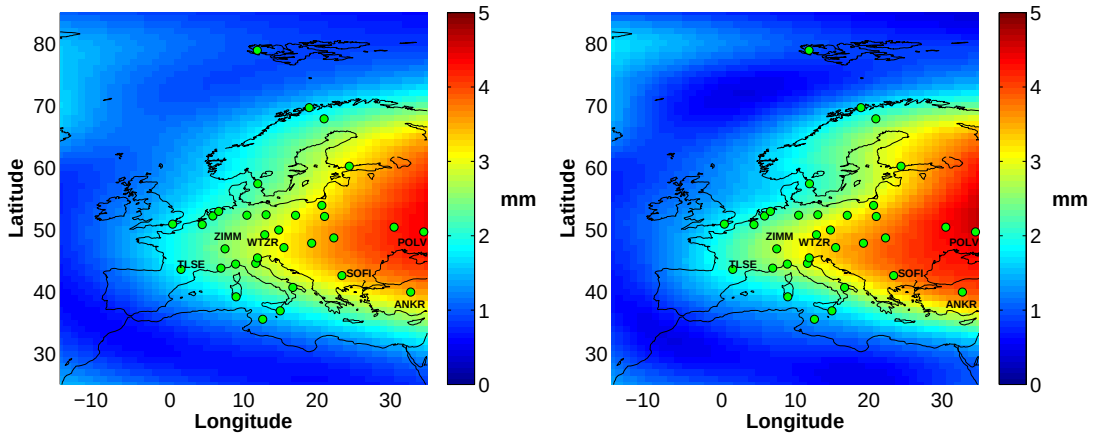

(a) 500 km *(b) 300 km*

Figure 4.27: *mean annual amplitudes of vertical deformations in Europe filtered by combination of Gaussian anisotropic and destriping filter*

After comparisons, we obtain the WRMS reduction and correlation coefficients of each station. For isotropic Gaussian filter, 20 of those stations show the filter with radius of 500 km has better results than 300 km, that indicates Gaussian isotropic or anisotropic filter with different radii shows nearly the same impact on loading deformations; For anisotropic Gaussian filter, 26 stations show the filter with radius of 300 km has larger WRMS reduction and correlation than with radius of 500 km. If the Gaussian isotropic filter is convolved with destriping filter, 31 stations with radius of 300 km perform better than those with radius of 500 km. The situation is the same when the anisotropic Gaussian smoothing combined with destriping filter.

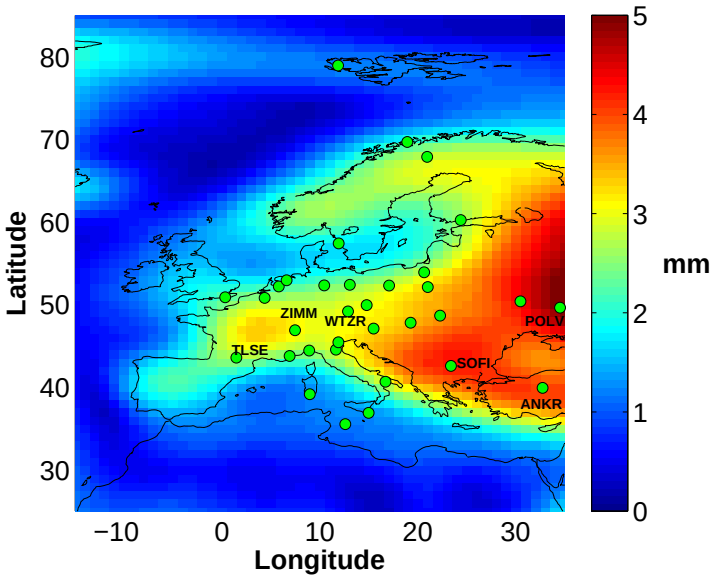

Figure 4.28: *mean annual amplitudes of vertical deformations in Europe filtered by stochastic filter*

Generally in geodesy, the distribution of gravity field on the Earth is not deterministic, we would like to know whether the stochastic filter is optimal for smoothing observations from GRACE. Thus, the Wiener filter is adopted here as stochastic filter. Besides the Gaussian group, the mean annual amplitudes filtered by Wiener filter would also be visualized in following figure 4.28.

Consequently, for the filter radius of both 500 km and 300 km, the combination of isotropic Gaussian filter and destriping filter seems to be the better choice since it has better performance than any others within Gaussian groups. If the Gaussian filter combined with destriping filter is applied to filter the GRACE data, the choice of radius of 300 km seems better than 500km, due to the larger WRMS reduction and higher correlation for most stations in loading deformations analysis, whatever the Gaussian filter is spatially isotropic or anisotropic.

To verify which type of filter is actually the optimal one, with the same radius, different type of filters are compared. For radius of 500 km, 29 of those stations filtered by isotropic Gaussian with destriping filter have larger WRMS reduction and correlation than by anisotropic smoothing with destriping filter; for radius of 300 km, 26 stations show that the isotropic Gaussian smoothing with destriping filter is more suitable than anisotropic smoothing with destriping filter. In Gaussian filter group, 42.5% stations indicate the isotropic Gaussian smoothing with radius of 300 km combined with destriping filter is the optimal one after comparisons.

To find out the optimal filter for GRACE data, the results from Gaussian filter group are compared additionally with stochastic filter. After comparisons, 50% stations filtered by stochastic filter show higher correlation than other filters (shown in figure 4.29), and 52.5% stations filtered by stochastic filter show larger WRMS reduction than other filters (shown in figure 4.30). The maximal difference of WRMS reduction within Gaussian filter group reaches 10% and normally the mean difference of the WRMS reduction among different combinations is only around 1%. However, compared with Gaussian group, the WRMS reduction can be improved by stochastic filter up to maximum 27%, and the average improvement is more than 3%. Thus, from the great improvement, we can conclude that the stochastic filter seems to be the optimal filter for most stations in European area.

Above all, if we choose the radius of 300 km, the anisotropic Gaussian filter or the combination of isotropic Gaussian with destriping filter should be adopted for GRACE data smoothing.

According to the statistical results, the stochastic filter is the optimal filter for more than 50% stations in Europe. For those stations shown in figure 4.28 (e.g. ANKR, POLV, SOFI, TLSE, WTZR, ZIMM) on the margin of area where deformations strongly happened, there is distinct improvement after stochastic filtering, compared with other types of Gaussian filters. The improvement is graphically illustrated by figure 4.31.

In brief, for global deformation derivation or inversion of loading, the isotropic Gaussian filter with radius of 300 km convolved with destriping filter can be simply applied for GRACE data

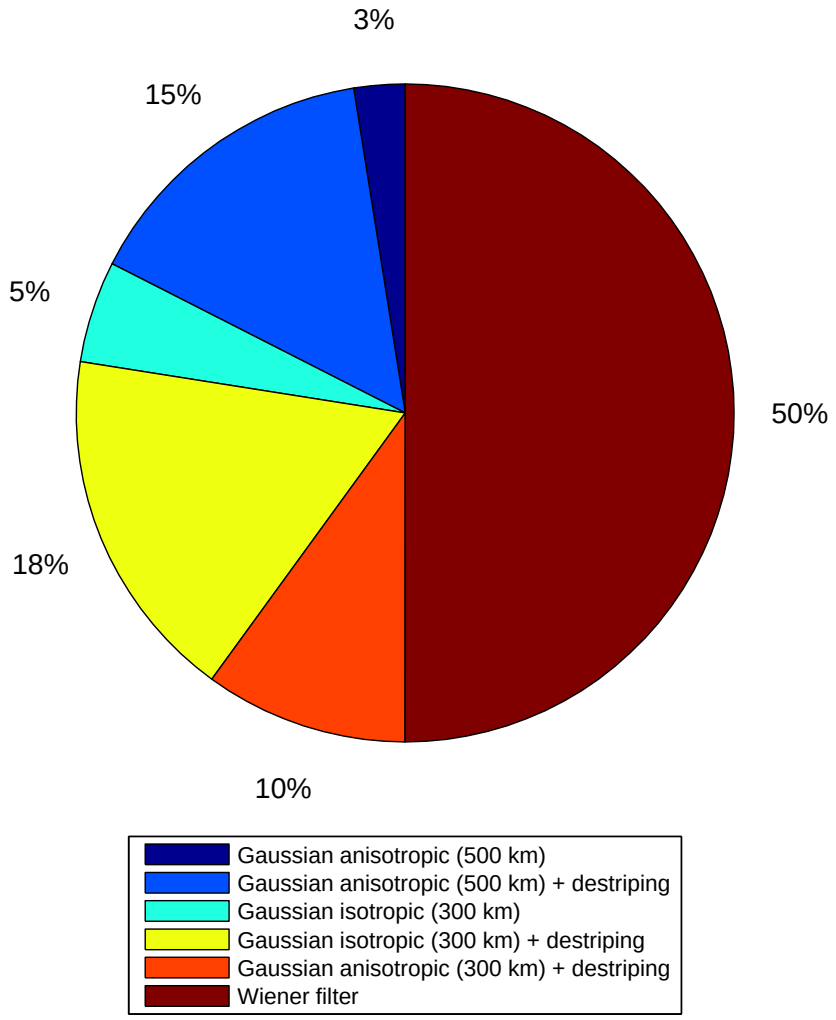

Figure 4.29: *Propotion of optimal filter for tested stations according to the correlation coefficients*

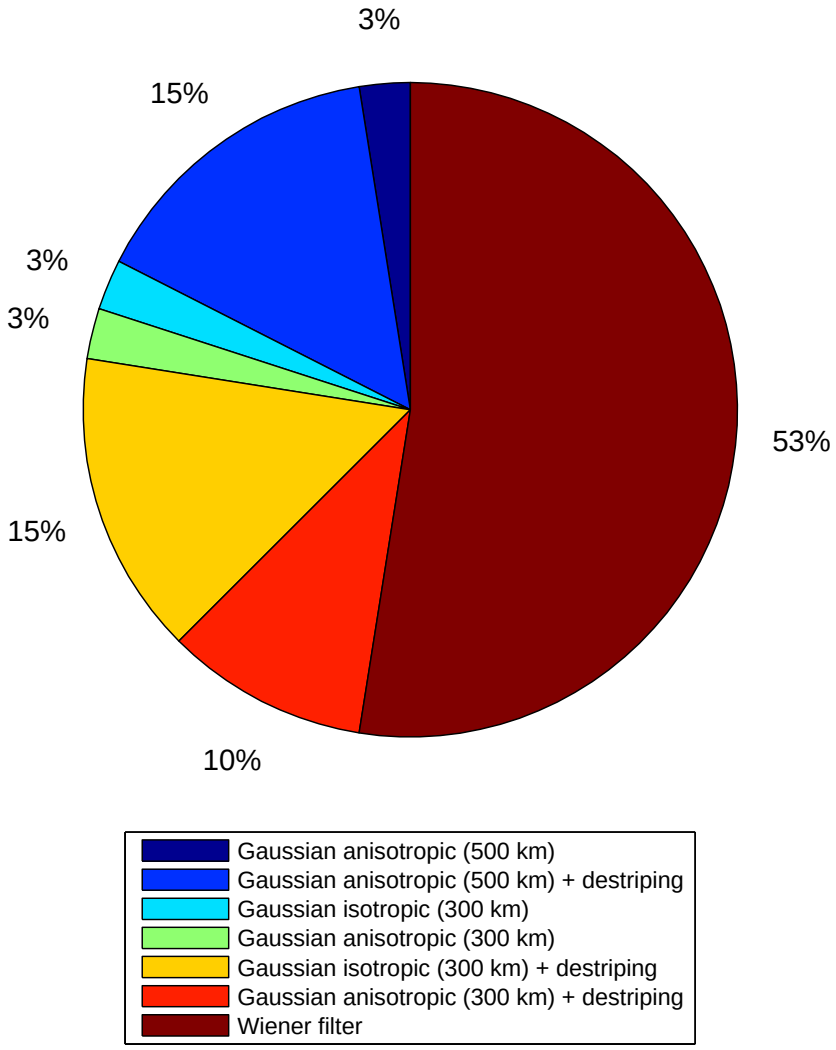

Figure 4.30: *Propotion of optimal filter for tested stations according to the WRMS reduction*

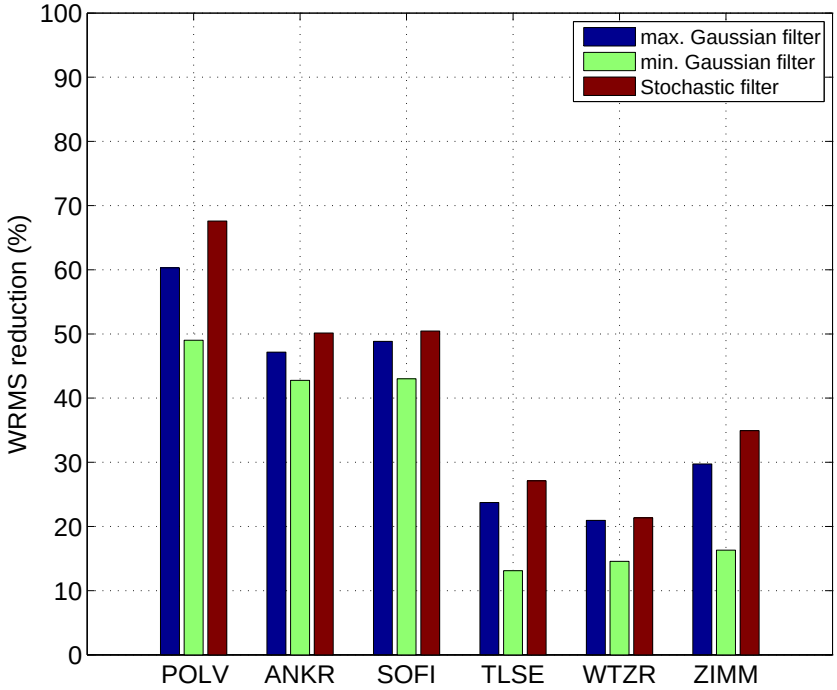

Figure 4.31: *Comparisons of stochastic filter with Gaussian filter group for 6 representative stations (POLV, ANKR, SOFI, TLSE, WTZR, ZIMM). The max.- and min.Gaussian filter denote the filters respectively with largest and smallest WRMS reduction in Gaussian filter group.*

smoothing. However, the stochastic filter is the optimal choice when we do the local loading analysis with several specified stations.

Chapter 5

Conclusion and Outlook

The objectives of this thesis have been proposed in Chapter 1.3.1, and the work which has been done so far can be summarized as follows:

- According to the theory in Chapter 3.1.2, the elastic surface displacements in vertical and horizontal directions have been mathematically derived from the spherical harmonic coefficient changes of gravity measured by GRACE. After the unification of spatial and time reference frame, the displacements derived from GRACE is able to be compared with 3D deformations observed by GPS.

- The disagreement of surface deformations between GRACE and GPS have been assessed by means of statistical methods in three different regions (Tibetan plateau, Danube basin, Great Lake area).

- With different kinds of filter combinations, the filter sensitivity test has been implemented in order to obtain the optimal filter combinations for GRACE deformation analysis.

Based on the work we have done in the thesis, the following conclusion would be drawn as below:

- With GRACE observations, it has been proved to have such capability to monitor the large-scale surface displacements induced by continental water loading variations, which can be derived from the time-variable gravity field of Earth. There is an implicit relation between mass redistribution and surface displacements, that is reflected by gravity change and then detected by GRACE mission.

- The deformations of all the stations in respective regions show strongly coherency with common annual patterns, such as on Tibetan plateau, in Danube basin, and in Great Lake area. This phenomenon proves the feasibility of regional surface loading deformation analysis.

- The deformation time series from both GPS and GRACE have obvious seasonal patterns, and especially in vertical direction, both of them show quite consistent annual harmonic deformations, that indicates these two independent geodetic observation systems are potential to estimate the surface loading variations. However, in horizontal direction, the deformation time series from GRACE do not behave so consistent with time series from GPS, and the magnitude of horizontal deformations is nearly one order smaller than vertical deformations. Therefore, the continental water loading variation affects principally on vertical component.
- Stochastic filter can retain more loading information to restore the true signal from GRACE raw data, especially for the stations on the margin of region where the loading deformations happened distinctly. On one hand, for global deformation derivation or inversion of loading, the isotropic Gaussian filter with radius of 300 km convolved with destriping filter can be simply applied for GRACE data smoothing; On the other hand, the stochastic filter is the optimal choice when we do the local loading deformation analysis with several specified stations, due to indeterministic property of surface load redistribution. However, because of the limited condition, the filter sensitivity test is only implemented regionally over a numbers of IGS stations in this thesis. And the methods for optimal filter test are still under debate.

Besides that, further discussion and outlook for our research are also necessary. Firstly, the inconsistency of spatial resolution for these two different observation systems should be primarily taken into account. To solve this problem, for example, the Principal Component Analysis (PCA) might be applied to evaluate the displacements on a surface not on discrete points. Other methods like assimilating with the observations from other geodetic systems are possible as well.

Also, the method for analyzing the horizontal deformations should be improved, in order to better interpret the large disagreement between GPS and GRACE at some stations.

The error sources should also be considered. For some stations, there is no clear annual repeating patterns from GPS time series, that reveals the GPS signals contain not only the annual terms but also semi-annual, interannual or nonseasonal components. It is preferable to remove these neglected influences if possible.

The stochastic filter implemented for GRACE data smoothing is isotropic Wiener filter, which is dependent only on degrees but not on orders. Furthermore, the anisotropic stochastic filter might also be implemented in GRACE data processing to compare with isotropic stochastic filter.

Bibliography

Bettadpur, S. (2007), 'Level-2 gravity field product user handbook', *GRACE 327* **734**.

Blewitt, G. (2003), 'Self-consistency in reference frames, geocenter definition, and surface loading of the solid Earth', *J. Geophys. Res.* **108**(B2), 2103–.

Blewitt, G., Lavallée, D., Clarke, P. and Nurutdinov, K. (2001), 'A New Global Mode of Earth Deformation: Seasonal Cycle Detected', *Science* **294**(5550), 2342–2345.

Case, K., Kruizinga, G. and Wu, S. (2002), 'GRACE level 1B data product user handbook', *JPL Publication D-22027* .

Dahle, C., Flechtner, F., Gruber, C., König, D., König, R., Michalak, G. and Neumayer, K. (2012), 'GFZ GRACE Level-2 Processing Standards Document for Level-2 Product Release 0005', *Scientific Technical Report-Data* **12**, –.

Davis, J. L., Elosegui, P., Mitrovica, J. X. and Tamisiea, M. E. (2004), 'Climate-driven deformation of the solid Earth from GRACE and GPS', *Geophys. Res. Lett.* **31**(24), L24605–.

De Linage, C., Hinderer, J. and Rogister, Y. (2007), 'A search for the ratio between gravity variation and vertical displacement due to a surface load', *Geophysical Journal International* **171**(3), 986–994.

Devaraju, B. and Sneeuw, N. (2012), Performance Analysis of Isotropic Spherical Harmonic Spectral Windows, *in* 'International Association of Geodesy Symposia', Vol. 137, Springer Berlin Heidelberg, pp. 105–110–.

Dong, D., Dickey, J. O., Chao, Y. and Cheng, M. K. (1997), 'Geocenter variations caused by atmosphere, ocean and surface ground water', *Geophys. Res. Lett.* **24**(15), 1867–1870.

Drinkwater, M. R., Haagmans, R., Muzi, D., Popescu, A., Floberghagen, R., Kern, M. and Fehringer, M. (2006), The GOCE gravity mission: ESA's first core Earth explorer, *in* 'Proceedings of the 3rd international GOCE user workshop', pp. 6–8.

Dunn, C., Bertiger, W., Franklin, G., Harris, I., Kruizinga, G., Meehan, T., Nandi, S., Nguyen, D., Rogstad, T. and Thomas, J. B. (2002), 'The instrument on NASA's GRACE Mission: Augmentation of GPS to achieve unprecedented gravity field measurements', pp. –.

Farrell, W. E. (1972), 'Deformation of the Earth by surface loads', *Rev. Geophys.* **10**(3), 761–797.

Flechtner, F. and Potsdam, G. (2007), AOD1B Product Description document for product releases 01 to 04 (rev. 3.1, april 13, 2007), Technical report, Technical report, GFZ.

Fu, Y. and Freymueller, J. T. (2012), 'Seasonal and long-term vertical deformation in the Nepal Himalaya constrained by GPS and GRACE measurements', *J. Geophys. Res.* **117**(B3), B03407–.

Fu, Y., Freymueller, J. T. and Jensen, T. (2012), 'Seasonal hydrological loading in southern Alaska observed by GPS and GRACE', *Geophys. Res. Lett.* **39**(15), L15310–.

Guo, J. Y., Duan, X. J. and Shum, C. K. (2010), 'Non-isotropic Gaussian smoothing and leakage reduction for determining mass changes over land and ocean using GRACE data', *Geophysical Journal International* **181**(1), 290–302.

Han, S.-C., Shum, C. K., Jekeli, C., Kuo, C.-Y., Wilson, C. and Seo, K.-W. (2005), 'Non-isotropic filtering of GRACE temporal gravity for geophysical signal enhancement', *Geophysical Journal International* **163**(1), 18–25.

Hofmann-Wellenhof, B. and Moritz, H. (2005), *Physical Geodesy*, Springer Wien New York.

Ilk, K., Flury, J., Rummel, R., Schwintzer, P., Bosch, W., Haas, C., Schröter, J., Stammer, D., Zahel, W. and Miller, H. (2005), 'Mass transport and mass distribution in the Earth system', *Contributions of the new generation of satellite gravity and altimetry missions to the geosciences* pp. –.

Jansen, M. J. F., Gunter, B. C. and Kusche, J. (2009), 'The impact of GRACE, GPS and OBP data on estimates of global mass redistribution', *Geophysical Journal International* **177**(1), 1–13.

Jekeli, C. (1981), 'Alternative methods to smooth the Earth's gravity field', *Rep.* **327**.

Klees, R., Revtova, E. A., Gunter, B. C., Ditmar, P., Oudman, E., Winsemius, H. C. and Savenije, H. H. G. (2008), 'The design of an optimal filter for monthly GRACE gravity models', *Geophysical Journal International* **175**(2), 417–432.

Kusche, J. (2007), 'Approximate decorrelation and non-isotropic smoothing of time-variable GRACE-type gravity field models', *Journal of Geodesy* **81**(11), 733–749–.

Kusche, J. and Schrama, E. J. O. (2005), 'Surface mass redistribution inversion from global GPS deformation and Gravity Recovery and Climate Experiment (GRACE) gravity data', *J. Geophys. Res.* **110**(B9), B09409–.

LeGrand, P. and Minster, J. (1999), 'Impact of the GOCE gravity mission on ocean circulation estimates', *Geophysical Research Letters* **26**(13), 1881–1884.

Lorenz, C. (2009), Applying stochastic constraints on time-variable GRACE data, Master's thesis, Institute of Geodesy, University of Stuttgart.

Mitrovica, J. X., Davis, J. L. and Shapiro, I. I. (1994), 'A spectral formalism for computing three-dimensional deformations due to surface loads', *J. Geophys. Res.* **99**(B4), 7057–7073.

Moriasi, D., Arnold, J., Van Liew, M., Bingner, R., Harmel, R. and Veith, T. (2007), 'Model evaluation guidelines for systematic quantification of accuracy in watershed simulations', *Transactions of the ASABE* **50**(3), 885–900.

Nahmani, S., Bock, O., Bouin, M.-N., Santamaria-Gomez, A., Boy, J.-P., Collilieux, X., Metivier, L., Panet, I., Genthon, P., de Linage, C. and Wöppelmann, G. (2012), 'Hydrological deformation induced by the West African Monsoon: Comparison of GPS, GRACE and loading models', *J. Geophys. Res.* **117**(B5), B05409–.

NASA (2002), GRACE Launch Press Kit, Technical report, NATIONAL AERONAUTICS AND SPACE ADMINISTRATION.

Nash, J. and Sutcliffe, J. (1970), 'River flow forecasting through conceptual models part i : A discussion of principles', *Journal of Hydrology* **10**(3), 282–290.

Reigber, C., Lühr, H. and Schwintzer, P. (2002), 'CHAMP mission status', *Advances in Space Research* **30**(2), 129–134.

Rietbroek, R., Fritsche, M., Brunnabend, S.-E., Daras, I., Kusche, J., Schröter, J., Flechtner, F. and Dietrich, R. (2012), 'Global surface mass from a new combination of GRACE, modelled OBP and reprocessed GPS data', *Journal of Geodynamics* **59-60**(0), 64–71.

Rodell, M. and Famiglietti, J. S. (2001), 'An analysis of terrestrial water storage variations in Illinois with implications for the Gravity Recovery and Climate Experiment (GRACE)', *Water Resour. Res.* **37**(5), 1327–1339.

Sasgen, I., Martinec, Z. and Fleming, K. (2006), 'Wiener optimal filtering of GRACE data', *Studia Geophysica et Geodaetica* **50**(4), 499–508–.

Seo, K.-W., Wilson, C. R., Famiglietti, J. S., Chen, J. L. and Rodell, M. (2006), 'Terrestrial water mass load changes from Gravity Recovery and Climate Experiment (GRACE)', *Water Resour. Res.* **42**(5), W05417–.

Sneeuw, N. (1994), 'Global spherical harmonic analysis by least-squares and numerical quadrature methods in historical perspective', *Geophysical Journal International* **118**(3), 707–716.

Sneeuw, N. (2006), *Physical geodesy*, Lecture notes.

Swenson, S. and Wahr, J. (2006), 'Post-processing removal of correlated errors in GRACE data', *Geophys. Res. Lett.* **33**(8), L08402–.

Tapley, B. D., Bettadpur, S., Watkins, M. and Reigber, C. (2004), 'The gravity recovery and climate experiment: Mission overview and early results', *Geophys. Res. Lett.* **31**(9), L09607–.

Tapley, J. Ries, S. B. D. M. F. S. P. (2007), The GGM03 Mean Earth Gravity Model from GRACE, Technical report, CSR.

Tesmer, V., Steigenberger, P., Dam, T. and Mayer-Gürr, T. (2011), 'Vertical deformations from homogeneously processed GRACE and global GPS long-term series', *Journal of Geodesy* **85**(5), 291–310–.

van Dam, T., Wahr, J. and Lavallee, D. (2007), 'A comparison of annual vertical crustal displacements from GPS and Gravity Recovery and Climate Experiment (GRACE) over Europe', *J. Geophys. Res.* **112**(B3), B03404–.

van Dam, T., Wahr, J., Milly, P., Shmakin, A., Blewitt, G., Lavallee, D. and Larson, K. (2001), 'Crustal displacements due to continental water loading', *Geophysical Research Letters* **28**(4), 651–654.

Velicogna, I. and Wahr, J. (2005), 'Greenland mass balance from GRACE', *Geophys. Res. Lett.* **32**(18), L18505–.

Wahr, J., Molenaar, M. and Bryan, F. (1998), 'Time variability of the Earth's gravity field: Hydrological and oceanic effects and their possible detection using GRACE', *J. Geophys. Res.* **103**(B12), 30205–30229.